Spectroscopic Characterization of the Atomic Hydrogen Energies and Densities and Carbon Species During Helium-Hydrogen-Methane Plasma CVD Synthesis of Single Crystal Diamond Films

Randell Mills*, Jayasree Sankar, Paresh Ray, Bala Dhandapani, Jiliang He

BlackLight Power, Inc.
493 Old Trenton Road
Cranbury, NJ 08512

Single crystal diamond films were synthesized on silicon substrates for the first time without diamond seeding by a microwave plasma reaction of a mixture of helium-hydrogen-methane (48.2/48.2/3.6%). The films were characterized by time of flight secondary ion mass spectroscopy (ToF-SIMS), X-ray photoelectron spectroscopy (XPS), Raman spectroscopy, and X-ray diffraction (XRD). It is proposed that He^+ served as a catalyst with atomic hydrogen to form an energetic plasma. CH, C_2, and C_3 emission were observed with significantly broadened H α, β, γ, and δ lines. The average hydrogen atom temperature of a helium-hydrogen-methane plasma was measured to be $120\text{-}140\,eV$ versus $\approx 3\,eV$ for pure hydrogen. Bombardment of the carbon surface by highly energetic hydrogen formed by the catalysis reaction may play a role in the formation of diamond. Then, by this novel pathway, the relevance of the $C-H-O$ tie line is eliminated along with other stringent conditions and complicated and inefficient techniques which limit broad application of the versatility and superiority of diamond thin film technology.

* Phone: 609-490-1090; Fax: 609-490-1066; E-mail: rmills@blacklightpower.com

key words: single crystal diamond films, CVD, helium-hydrogen-methane microwave plasma, spectroscopic characterization, energetic hydrogen mechanism

I. INTRODUCTION

Diamond has some of the most extreme physical properties of any material such as outstanding mechanical strength, optical transparency, high thermal conductivity, high electron mobility, and unique chemical properties [1]. Thus, a variety of possible applications are envisioned for diamond materials. Yet, its practical use in applications has been limited due to its scarcity, expense, and immalleability. The development of techniques for depositing thin films of synthetic diamonds on a variety of substrates has enabled the exploitation of diamond's superlative properties in many new and exciting applications. These include cutting tools, thermal management of integrated circuits, optical windows, high temperature electronics, surface acoustic wave (SAW) filters, field emission displays, electrochemical sensors, composite reinforcement, microchemical devices and sensors, and particle detectors [1]. But, the fundamental impediment facing the technology at the present is insufficient growth rate of high-quality diamond.

Synthetic diamond was initially commercially produced as single crystals using the high-pressure high-temperature (HPHT) growth technique [1] wherein graphite is compressed in a hydraulic press to tens of thousands of atmospheres, heated to over 2000 K, and left until diamond crystallizes. Recent novel HPHT methods which have been largely unsuccessful, except for the production of nanocrystals by Orwa et. al. [2], are based on attempts to use high energy ion implantation to bury carbon deep in metals or fused silica to take advantage of the large confining pressures there. More versatile thin films have been produced by an addition-of-one-atom-at-a-time approach using chemical vapor deposition (CVD) techniques. All CVD techniques for producing diamond films require activation of the gaseous carbon-containing precursor molecules. To promote diamond over graphite growth, the precursor gas is usually CH_4 that is diluted in excess hydrogen that is typically 99% of the reactant mixture, and the temperature of the substrate is usually maintained in excess of 700°C. Activation may be achieved thermally using a hot filament, gas discharge such as DC, RF, or microwave discharges, or a combustion flame such as an oxyacetylene torch [1].

Although the mechanism of diamond growth on a seed of diamond is still somewhat of a mystery, it is believed to be based on the extraction of H of a CH terminal bond to form a dangling carbon center to which CH_3 reacts. A carbon-carbon bond forms between adjacent methyl groups, and the hydrogen is gradually extracted, probably by H forming H_2. The further preferential degradation of graphitic carbon over diamond carbon by hydrogen permits diamond growth [1]. H may also be required to decrease the concentration of gas phase unsaturated hydrocarbons.

More recent advances of diamond formation have been towards developing methods to grow diamond at low temperatures (< 500°C rather than 700°C) such that diamond films can be grown on a wider range of substrate materials of commercial importance with low melting points such as plastics, aluminum, some glasses, nickel, steel and electronics materials such as *GaAs*. Many gas mixtures have been investigated to achieve this goal including ones containing some halogens, presumably substituting for the role played by H [3]. More common mixtures have different combinations of H_2, CH_4, O_2, CO_2, and CO [3]. Quite successful diamond film growth has been achieved at temperatures as low as 180°C using gas mixtures of CH_4 mixed with CO_2 or CO in microwave plasma deposition reactors wherein an optimal rate is obtained when the gas ratio is about 50/50%. Although the concentration of H_2 in the activated gas mixture is approximately half that seen in the CH_4/ H_2 mixtures [4], the CO_2- CH_4 and CO- CH_4 systems are unique in that hydrogen is low compared to the excess needed in other systems presumably because oxygen species such as O_2, O, and OH in the CO_2- CH_4 and CO- CH_4-system plasmas perform the same role as H in the CH_4- H_2-system plasmas. Recent molecular beam mass spectroscopy investigations of the CO_2- CH_4 system indicate the incorporation of CH_3 at a dangling carbon bond is the most probable mechanism as in the case of the CH_4- H_2 system. However, the species that extracts H may not be an oxygen species. Rather, CO may activate the surface by extracting a terminating H [5].

Empirically it is known that only narrow set of ratios of O, C, and H result in diamond formation. Using the combined data from over 70 diamond deposition experiments, Bachmann et al. produced a $C-H-O$

phase diagram for diamond deposition which showed that low pressure diamond synthesis is only possible within a very narrow well-defined domain centered on a line called the $C-H-O$ tie line [6-7]. A consequence of this analysis was that the exact nature of the plasma gases was unimportant for most CVD processes; rather, the relative ratios of O, C, and H controlled the deposition.

It was previously reported that a novel highly stable surface coating SiH which comprised high binding energy hydride ions was synthesized by microwave plasma reaction of mixture of silane, hydrogen, and helium wherein it was proposed that He^+ served as a catalyst with atomic hydrogen to form the highly stable hydride ions [8]. The novel silicon hydride was identified by time of flight secondary ion mass spectroscopy (ToF-SIMS) and X-ray photoelectron spectroscopy (XPS). ToF-SIMS identified the coatings as hydride by the large SiH^+ peak in the positive spectrum and the dominant H^- in the negative spectrum. XPS identified the H content of the SiH coatings as hydride ions corresponding to peaks at 11, 43, and 55 eV. The silicon hydride surface was remarkably stable in air for long duration exposure as shown by XPS.

In the quest for low temperature diamond synthesis, CH_4 was substituted for SiH_4 in the helium-hydrogen microwave reaction which formed novel SiH. We report for the first time the deposition of single crystal diamond films on silicon-wafers by a helium-hydrogen-methane (48.2/48.2/3.6%) microwave plasma maintained with an Evenson cavity without diamond seeding or abrasion that provides seed crystals [9]. After the plasma processing reaction, the surface was characterized by ToF-SIMS, XPS, Raman spectroscopy, and X-ray diffraction (XRD). In order to understand the role of the helium-hydrogen plasma, it was characterized by recording the line broadening of the 656.3 nm Balmer α line to determine the excited hydrogen atom energy. The visible spectrum was also recorded to determine the relative concentrations of species in the gaseous reaction mixture.

II. EXPERIMENTAL

Synthesis

Diamond films were grown on silicon wafer substrates by their exposure to a low pressure $He\text{-}H_2\text{-}CH_4$ microwave plasma. The experimental set up comprising a microwave discharge cell operated under flow conditions is shown in Figure 1. A silicon wafer substrate (0.5 X 0.5 X 0.05 cm, Silicon Quest International, silicon (100), boron doped) cleaned by heating to 700°C under vacuum was placed about 2 cm off center inside of a quartz tube (1.2 cm in diameter by 25 cm long) with vacuum valves at both ends. The tube was center-fitted with an Opthos coaxial microwave cavity (Evenson cavity) and connected to the gas/vacuum line. The quartz tube and vacuum line were evacuated for 2 hours to remove any trace moisture or oxygen and residual gases. The reaction mixture of helium-hydrogen-methane (48.2/48.2/3.6%) was flowed through the quartz tube at a total pressure of 3 Torr maintained with a total gas flow rate of 62.25 sccm controlled by two mass flow controllers with readouts. The cell pressure was monitored by an absolute pressure gauge. The methane flow at one mass flow controller was 2.25 sccm and a helium-hydrogen flow of 60 sccm was controlled by a second mass flow controller from a 50/50% premixture. In separate experiments, the helium-hydrogen premixed gas was varied from (90/10%) to (50/50%). Since the best diamond film results were obtained with the (50/50%) mixture, only these results will be presented.

The microwave generator shown in Figure 1 was an Opthos model MPG-4M generator (Frequency: 2450 MHz). The microwave plasma was maintained with a 40 W (forward)/2 W (reflected) power for about 12-16 hrs. The substrate was at the cool edge of the plasma glow region. The wall temperature at this position was about 300°C. A thick (~100 μm) crystalline, shiny coating formed on the substrate and the wall of the quartz reactor. The quartz tube was removed and transferred to a drybox with the samples inside by closing the vacuum valves at both ends and detaching the tube from the vacuum/gas line. The coated silicon wafer substrate was mounted on XPS and ToF-SIMS sample holders under an argon atmosphere in order to prepare samples for the corresponding analyses. Controls for XPS analysis comprised a cleaned commercial silicon wafer (Silicon Quest International, silicon (100), boron doped) and known standards: (a) single crystal diamond, (b) diamond film, (c) glassy carbon, (d) pyrolytic graphite, (e) mineral graphite, and (f)

HDLC (hydrogenated diamond-like carbon). The control for ToF-SIMS analysis comprised a cleaned commercial silicon wafer (Silicon Quest International, silicon (100), boron doped). The coated substrate was also sent for Raman analysis (Charles Evans & Associates, Sunnyvale, CA and Jobin Yvon Inc., Edison, New Jersey) and XRD analysis (IC Laboratories, Amawalk, NY).

ToF-SIMS Characterization

A cleaned commercial silicon wafer before and after plasma treatment to form a diamond film coating were characterized using a Physical Electronics TRIFT ToF-SIMS instrument. The primary ion source was a pulsed $^{69}Ga^{+}$ liquid metal source operated at 15 keV. The secondary ions were exacted by a ± 3 keV (according to the mode) voltage. Three electrostatic analyzers (Triple-Focusing-Time-of-Flight) deflect them in order to compensate for the initial energy dispersion of ions of the same mass. The 400 pA dc current was pulsed at a 5 kHz repetition rate with a 7 ns pulse width. The analyzed area was $60\mu m$ x $60\mu m$ and the mass range was 0-1000 AMU. The total ion dose was $7X10^{11}\ ions/cm^2$, ensuring static conditions. Charge compensation was performed with a pulsed electron gun operated at 20 eV electron energy. In order to remove surface contaminants and expose a fresh surface for analysis, the samples were sputter-cleaned for 30 s using a $80\mu m$ x $80\mu m$ raster, with 600 pA current, resulting in a total ion dose of $10^{15}\ ions/cm^2$. Three different regions on each sample of $60\mu m$ x $60\mu m$ were analyzed. The positive and negative SIMS spectra were acquired. Representative post sputtering data is reported. The ToF-SIMS data were treated using 'Cadence' software (Physical Electronics), which calculates the mass calibration from well-defined reference peaks.

XPS Characterization

A series of XPS analyses were made on the samples using a Scienta 300 XPS Spectrometer at Lehigh University, Bethlehem, PA. The fixed analyzer transmission mode and the sweep acquisition mode were used. The Aluminum X-ray incidence angle was 15°. The step energy in the survey scan was $0.5\,eV$, and the step energy in the high resolution scan was $0.15\,eV$. In the survey scan, the time per step was 0.4 seconds, and

the number of sweeps was 4. In the high resolution scan, the time per step was 0.3 seconds, and the number of sweeps was 30. $C\,1s$ at 284.6 eV was used as the internal standard.

Raman Spectroscopy

Experimental and control samples were analyzed by Charles Evans & Associates, Sunnyvale, CA. Raman spectra were obtained with a LABRAM spectrometer (Dilor of Jobin Yvon) with a Spectrum One CCD (charge coupled device) detector (Spex and Jobin Yvon) that was air and Peltier cooled. An Omnichrome HeNe laser (Melles Griot) with the light wavelength of 632.817 nm was used as the excitation source. The spectra were taken at ambient conditions and the samples were placed under a Raman microscope (Olympus BX40). Spectra of the film samples were acquired using the following condition: the laser power at the sample was 4 to 8 mW, the slit width of the monochromator was 100 μm which corresponds to a resolution of 3 cm^{-1}, the detector exposure time was 20 min., and 3 scans were averaged.

Experimental and control samples were also analyzed by Jobin Yvon Inc., Edison, New Jersey. Raman spectra were obtained with a LabRam HR system (Jobin Yvon Inc.) with a built in microscope. The spectrometer had two interchangeable gratings with 1800 gr/mm, blazed at 500 nm, and was equipped with a liquid nitrogen-cooled CCD detector (1024 X 256, BI, UV coated). A helium-cadmium laser with the light wavelength of 325 nm was used as the excitation source. The spectra were taken at ambient conditions, and the samples were mounted under the Raman microscope. Spectra of the film samples were acquired at 3 second integration using the following condition: the laser power at the sample was 15 mW and the slit width of the monochromator was 500 μm which corresponds to a resolution of 2.5 cm^{-1}.

Characterization by X-ray Diffraction (XRD)

The XRD patterns were obtained by IC Laboratories (Amawalk, NY) using a Phillips 547 Diffractometer tuned for $Cu\,K_\alpha$ (1.540590 Å) radiation generated at 45 kV and 35 mA. The sample was scanned from 10 to 100 2-theta (2θ) with a step size of 0.02° and 1 second per step.

Visible Spectroscopy and Balmer Line Broadening Measurements

The width of the 656.3 nm Balmer α line, 486.1 nm Balmer β line, 434.0 nm Balmer γ line, and 410.2 nm Balmer δ line emitted from hydrogen alone, xenon-hydrogen mixture (90/10%), helium-hydrogen mixture (90/10%), hydrogen-methane mixture (10-50/90-50%), and helium-hydrogen-methane mixture (48.2/48.2/3.6%) microwave discharge plasmas maintained in the microwave discharge cell shown in Figure 1 was measured with a high resolution visible spectrometer capable of a resolution of $\pm 0.006\,nm$ according to methods given previously [10-11]. The spectra were recorded over the regions (410.05 nm-410.35 nm, 433.85-434.35 nm, 485.90-486.40 nm, and 656.0-657.0 nm). The total flow rate was controlled at 62.25 sccm using one mass flow controller for hydrogen alone and two in the case of a mixture of two gases. In the case of the helium-hydrogen-methane mixture, the methane flow at one mass flow controller was 2.25 sccm and the helium-hydrogen flow of 60 sccm was controlled by a second mass flow controller from a 50/50% mixture. The total pressure was 3 Torr, and the input power to the plasma was set at 40 W. The 667.816 nm He I line width was also recorded with the high resolution ($\pm 0.006\,nm$) visible spectrometer on helium-hydrogen (90/10%) and helium microwave discharge plasmas. The visible spectrum was also recorded on the helium-hydrogen-methane mixture (48.2/48.2/3.6%) microwave discharge plasma.

The electron density was determined using a Langmuir probe according to the method given previously [12].

III. RESULTS

ToF-SIMS

The positive ion ToF-SIMS spectra of a cleaned commercial silicon wafer before and after being coated with a carbon film are shown in Figures 2 and 3, respectively. The positive ion spectrum of the control was dominated by Si^+, oxides $Si_xO_y^+$, and hydroxides $Si_x(OH)_y^+$; whereas, that of the carbon film sample contained no silicon containing fragments. Rather, a large H^+ peak and trace hydrocarbon fragments $C_xH_y^+$ were observed. The $m/e = 69$ peak was due to the Ga^+.

The negative ion ToF-SIMS spectra of a cleaned commercial silicon wafer before and after being coated with a carbon film are shown in Figures 4 and 5, respectively. The control spectrum was dominated by oxide (O^-) and hydroxide (OH^-); whereas, spectrum of the carbon film was dominated by hydride ion (H^-) and carbon ion (C^-). Very little oxide (O^-) or hydroxide (OH^-) was observed. An exceptional feature was the multimeric carbon clusters C_x^- at $m/e = 12,24,36,48,60,72,96,108,120$.

XPS

A survey spectrum was obtained over the region $E_b = 0\ eV$ to $1200\ eV$. The primary element peaks allowed for the determination of all of the elements present. The XPS survey scan of a cleaned commercial silicon wafer before and after being coated with a carbon film are shown in Figures 6 and 7, respectively. The major peaks identified in the XPS spectrum of the control sample were $O\,1s$ at 533.0 eV, trace $C\,1s$ at 284.6 eV, dominant $Si\,2s$ at 152.4 eV and $Si\,2p_{3/2}$ at 101.9 eV. Whereas, the carbon film sample comprised only carbon and trace silicon and oxygen contamination as indicated by the trace $O\,1s$ peak at 532.9 eV, the trace $Si\,2s$ at 153.2 eV and $Si\,2p_{3/2}$ at 102.2 eV, and the dominant $C\,1s$ peak at 284.6 eV.

The high resolution XPS spectra (0-35 eV) of the valence band region of (a) single crystal diamond, (b) diamond film, (c) glassy carbon, (d) pyrolytic graphite, (e) mineral graphite, and (f) HDLC are shown in Figure 8 [13]. The corresponding XPS spectrum of the carbon film sample is shown in Figure 9. The film had a sharp peak at 13.2 eV and a broad peak at 17.4 eV which matched the peak energies of single crystal diamond rather than that of the other forms of carbon which were observed at higher binding energies. No $O\,2s$ peak was also observed in the region of 23 eV as shown in Figure 9.

The high resolution XPS spectra (280-340 eV) of the $C\,1s$ energy loss region of (a) single crystal diamond, (b) diamond film, (c) glassy carbon, (d) pyrolytic graphite, (e) mineral graphite, and (f) HDLC are shown in Figure 10 [13]. The corresponding XPS spectrum of the carbon film sample is shown in Figure 11. Single crystal diamond, diamond film, and HDLC have an energy loss feature which begins at about 290 eV which is at a higher energy than that of the other possible forms of

carbon as shown in Figure 10. The closest match to the shape of the energy loss feature of the carbon film is single crystal diamond to which the film was assigned.

Raman

The Raman spectrum of the corresponding region of the diamond film that was analyzed by ToF-SIMS and XPS is shown in Figure 12. Extensive curve fit analysis was performed. The peak positions, full-width-half-maximum (FWHM), and peak areas were calculated by Gaussian curve fitting the baseline corrected spectrum. The diamond band was observed at 1323.5 cm^{-1}, with a FWHM of 19.6 cm^{-1}. The diamond peak width of less that 20 cm^{-1} identified the film as having single crystal diamond [14]. In addition to the diamond band, the D-band, G-band of diamond-like carbon (DLC), and G-band of graphite were observed at 1327.0 cm^{-1} with a FWHM of 76 cm^{-1}, 1484.0 cm^{-1} with a FWHM of 130.2 cm^{-1}, and 1591.6 cm^{-1} with a FWHM of 46.5 cm^{-1}, respectively.

The ratio of the areas of the diamond peak to G-band of graphite, $\frac{I_D}{I_G}$, is considered an indirect measure of carbon $\frac{sp^3}{sp^2}$ bonding ratio. The ratio $\frac{I_D}{I_G}$ was 0.73. The Raman spectrum confirmed the XPS results that the film comprised diamond. Based on quantitative studies [15-16], we estimate that the diamond composition of the films was well over 50%.

The Raman spectrum was repeatable as shown in Figure 13. A diamond band was observed at 1332 cm^{-1} for a second diamond film formed by helium-hydrogen-methane microwave discharge plasma (48.2/48.2/3.6%) CVD. In addition, the G-band of graphite was observed at 1580.

XRD

The X-ray Diffraction (XRD) pattern of the diamond film for 2θ = 10° to 100° is shown in Figure 14. The dominant peaks were due to silicon of the substrate. Diamond peaks were observed at 2θ = 43.9° (111) and 75.3° (220) [17-18]. Additional peaks other than silicon and diamond corresponded to DLC.

Visible Spectrum and Line Broadening

The visible spectrum (275-700 nm) recorded on a helium-hydrogen-methane (48.2/48.2/3.6%) microwave discharge plasma is shown in Figure 15. The H α, β, γ, and δ lines observed at 656.3 nm, 486.2 nm, 434.1 nm and 410.2 nm, respectively, were significantly broadened as discussed *infra*. He I emission lines were observed at 667.8 nm and 468.57 nm. A progression of *CH* vibrational peaks were observed at 389 nm and 431 nm. The C_3 band was observed at 405.4 nm, and the C_2 Swan band ($A\,^3\Pi_g \rightarrow X\,^3\Pi_u$), $\Delta\upsilon = -1$ was observed at 468.2 nm. The $H : C_2$, $CH : C_2$, and $CH : C_3$ peak intensity ratios were similar to those reported by Elliott et al. [3] that were correlated with the optimal conditions for diamond film quality and growth rate during diamond CVD using CH_4-CO_2 plasmas.

The Doppler-broadened line shape for atomic hydrogen has been studied on many sources such as hollow cathode [19-20] and rf [21-22] discharges. The method of Videnovic et al. [19] was used to calculate the energetic hydrogen atom densities and energies from the width of the 656.3 nm Balmer α line emitted from microwave discharge plasmas of hydrogen compared with each of xenon-hydrogen (90/10%) and helium-hydrogen (90/10%) as shown in Figures 16-17, respectively. Gigosos et al. [23] have published a literature review of this method. The average helium-hydrogen Doppler half-width was not appreciably changed with pressure. The corresponding energy of $180\text{-}210\,eV$ and the number density of $5\,X\,10^{14} \pm 20\%\ atoms/cm^3$, depending on the pressure, were significant compared to only $2-3\,eV$ and $7\,X\,10^{13} \pm 20\%\ atoms/cm^3$ for pure hydrogen, even though 10 times more hydrogen was present. Xenon did not serve as a catalyst, and the plasma was much less energetic. Xenon-hydrogen showed no excessive broadening corresponding to an average hydrogen atom temperature of $2-3\,eV$, and the atom density was also low, $3\,X\,10^{13} \pm 20\%\ atoms/cm^3$.

Significant broadening was also observed for the helium-hydrogen-methane (48.2/48.2/3.6%) plasma as shown in Figure 18. The average hydrogen atom temperature and density were high, $120\text{-}140\,eV$ and $3\,X\,10^{14} \pm 20\%\ atoms/cm^3$, respectively, compared to $2-3\,eV$ and $2\,X\,10^{13} \pm 20\%\ atoms/cm^3$ for a hydrogen-methane plasma. The percentage of

hydrogen was varied from 10 to 50% with methane comprising the other component of the mixture. No broadening was observed with any of these plasmas.

Only the hydrogen lines were broadened. For example, the 667.816 nm He I line width was also recorded with the high resolution ($\pm 0.006\ nm$) visible spectrometer on helium-hydrogen (90/10%) and helium microwave discharge plasmas. No broadening was observed in either case. Whereas, in each case, the broadening of the H β, γ, and δ lines were equivalent to that of the H α line.

We have assumed that Doppler broadening due to thermal motion was the dominant source to the extent that other sources may be neglected. This assumption was confirmed when each source was considered. In general, the experimental profile is a convolution of two Doppler profiles, an instrumental profile, the natural (lifetime) profile, Stark profiles, van der Waals profiles, a resonance profile, and fine structure. The electron density recorded with a Langmuir probe was five orders of magnitude too low for detectable Stark broadening, and the contribution from each remaining source was determined to be below the limit of detection [10-11].

IV. DISCUSSION

Diamond films were deposited on silicon substrates by the reaction product of a low pressure $He\text{-}H_2\text{-}CH_4$ (48.2/48.2/3.6%) microwave discharge plasma. The ToF-SIMS of the carbon film showed carbon clusters, and the XPS matched single crystal diamond which was confirmed by the Raman diamond peak at 1323.5 cm^{-1} with a FWHM of less than 20 cm^{-1}. Diamond is proposed to form from CH_4 by the catalytic reaction of He^+ with atomic hydrogen which forms an energetic plasma which was measured to have extraordinarily fast H.

In the previously developed $CH_4\text{-}H_2$-system and variations thereof, diamond formation occurs within a small domain about the $C-H-O$ tie line. Stringent conditions of a large excess of hydrogen, diamond seeding, and an elevated temperature are required. Similarly, in the $CO_2\text{-}CH_4$ system, diamond only formed within a range of a few percent from a 50/50% mixture. We observed for the first time that diamond was very

reproducibly formed from a CH_4 carbon source with a helium-hydrogen plasma without the requirements of diamond seeding, an elevated temperature, or an excess of hydrogen, or any particular former set of stringent conditions. Thus, a dramatic breakthrough in thin film diamond deposition has been shown.

The mechanism may be based on energetic hydrogen formed in the plasma reaction. Diamond and DLC are metastable materials; thus, continuous bombardment of the surface with energetic species that produce thermal and pressure spikes at the growth surface is required for deposition of diamond, DLC, and related films [24]. By quenching a beam of C^+ ions accelerated in an ultrahigh vacuum to a negatively biased substrate, Aisenberg and Chabot [25] were able to deposit DLC films for the first time. Rather than resulting in commercially useful processes, subsequently developed beam-type and sputtering production methods are essentially used for research. Exemplary methods discussed by Grill and Myerson [26] are single low-energy beams of carbon ions, dual ion beams of carbon and argon, ion plating, RF sputtering or ion-beam sputtering from carbon/graphite targets, vacuum-arc discharges, and laser ablation. Using sputter deposition, amorphous DLC coatings can be prepared at low temperature due to high ion bombardment during the deposition of carbon. The absence of ion bombardment during carbon deposition leads to soft, conductive carbon films with no diamond-like properties. It has been shown that films with diamond-like properties are produced at ion energies of about 100 eV [27-28].

Energetic species such as fast H formed in the helium-hydrogen microwave plasma that showed extraordinary Balmer α line broadening corresponding to an average hydrogen atom temperature of $120\text{-}140\,eV$ may be the basis of the formation of the diamond film from CH_4. Without diamond seeding, production of single crystal diamond films on heterogeneous substrates was achieved under relatively low temperature, nonstringent conditions.

ACKNOWLEDGMENTS

Thanks to A. Miller of Lehigh University for XPS analysis and very useful discussions, and V. Pajcini of Charles Evans & Associates and O. Klueva of Jobin Yvon Inc. for Raman analysis and useful discussions.

REFERENCES

1. P. W. May, "Diamond thin films: a 21 st-century material", Phil. Trans. R. Soc. Lond. A, Vol. 358, (2000), pp. 473-495.
2. J. O. Orwa, S. Prawer, D. N. Jamieson, J. L. Peng, J. C. McCallum, K. W. Nugent, Y. J. Li, L. A. Bursill, "Diamond nanocrystals formed by direct implantation of fused silica with carbon", Journal of Applied Physics, Vol. 90, No. 6, (2001), pp. 3007-3018.
3. M. A. Elliott, P. W. May, J. Petherbridge, S. M. Leeds, M. N. R. Ashfold, W. N. Wang, "Optical emission spectroscopic studies of microwave enhanced diamond CVD using CH_4/ CO_2 plasmas", Diamond and Related Materials, Vol. 9, (2000), pp. 311-316.
4. J. R. Petherbridge, P. W. May, S. R. J. Pearce, K. N. Rosser, M. N. R. Ashfold, "Low temperature diamond growth using CO_2/ CH_4 plasmas: Molecular beam mass spectroscopy and computer simulation investigations", Journal of applied Physics, Vol. 89, No. 2, Jan. 15, (2001), pp. 1484-1492.
5. J. Petherbridge, P. W. may, S. R. J. Pearce, K. N. Rosser, M. N. R. Ashfold, "Molecular beam mass spectrometry investigations of low temperature diamond growth using CO_2/ CH_4 plasmas", Diamond and Related Materials, Vol. 10, (2001), pp. 393-398.
6. P. K. Bachmann, D. Leers, H. Lydtin, D. U. Wiechert, Diamond and Related Materials, Vol. 1, No. 1, (1991), p. 1.
7. P. K. Bachmann, H. G. Hagemann, H. Lade, D. Leers, F. Picht, D. U. Wiechert, Mater. Res. Soc. Proc., Vol. 339, (1994), p. 267.
8. R. L. Mills, B. Dhandapani, J. He, "Highly Stable Amorphous Silicon Hydride", J of Materials Research, submitted.
9. J. H. D. Rebello, D. L. Straub, V. V. Subramaniam, "diamond growth from a CO/ CH_4 mixture by laser excitation of CO: Laser excited chemical vapor deposition", J. Appl. Phys., Vol. 72, No. 3, (1992), pp. 1133-1136.

10. R. L. Mills, P. Ray, "Substantial Changes in the Characteristics of a Microwave Plasma Due to Combining Argon and Hydrogen", New Journal of Physics, www.njp.org, Vol. 4, (2002), pp. 22.1-22.17.
11. R. L. Mills, P. Ray, B. Dhandapani, J. He, "Comparison of Excessive Balmer α Line Broadening of Glow Discharge and Microwave Hydrogen Plasmas with Certain Catalysts", J. of Applied Physics, submitted.
12. D. Barton, J. W. Bradley, D. A. Steele, and R. D. Short, "investigating radio frequency plasmas used for the modification of polymer surfaces," J. Phys. Chem. B, Vol. 103, (1999), pp. 4423-4430.
13. Provided by A. Miller, Zettlemoyer Center for Surface Studies, Sinclair Laboratory, Lehigh University Bethlehem, PA.
14. M. G. Donato, G. Faggio, M. Marinelli, G. Messina, E. Milani, A. Paoletti, S. Santangelo, A. Tucciarone, G. Verona Rinati, Diamond and Related Materials, Vol. 10, (2001), pp. 1788-1793.
15. S. M. Leeds, T. J. Davis, P. W. May, C. D. O. Pickard, M. N. R. Ashfold, "Use of different wavelengths for analysis of CVD diamond by laser Raman Spectroscopy", Diamond and Related Materials, Vol. 7, (1998), pp. 233-237.
16. K. W. R. Gilkes, S. Prawer, K. W. Nugent, J. Robertson, H. S. Sands, Y. Lifshitz, X. Shi, "Direct quantitative detection of the sp^3 bonding in diamond-like carbon films using ultraviolet and visible Raman spectroscopy", Journal of Applied Physics, Vol. 87, No. 10, (2000), pp. 7283-7289.
17. P. D. Ownby, X. Yang, J. Liu, J. Am. Ceram. Soc., Vol. 75, (1992), p. 1876.
18. J. Thewlis, A. R. Davey, Philos. Mag., Part B, Vol. 1, (1956), p. 409.
19. I. R. Videnovic, N. Konjevic, M. M. Kuraica, "Spectroscopic investigations of a cathode fall region of the Grimm-type glow discharge", Spectrochimica Acta, Part B, Vol. 51, (1996), pp. 1707-1731.
20. S. Alexiou, E. Leboucher-Dalimier, "Hydrogen Balmer-α in dense plasmas", Phys, Rev. E, Vol. 60, No. 3, (1999), pp. 3436-3438.
21. S. Djurovic, J. R. Roberts, "Hydrogen Balmer alpha line shapes for hydrogen -argon mixtures in a low-pressure rf discharge", J. Appl. Phys., Vol. 74, No. 11, (1993), pp. 6558-6565.

22. S. B. Radovanov, K. Dzierzega, J. R. Roberts, J. K. Olthoff, Time-resolved Balmer-alpha emission from fast hydrogen atoms in low pressure, radio-frequency discharges in hydrogen", Appl. Phys. Lett., Vol. 66, No. 20, (1995), pp. 2637-2639.
23. M. A. Gigosos, V. Cardenoso, "New plasma diagnosis tables of hydrogen Stark broadening including ion dynamics", J. Phys. B: At. Mol. Opt. Phys., Vol. 29, (1996), pp. 4795-4838.
24. C. Weissmantel, *Thin Films from Free Atoms and Molecules*, K. J. Klabunde, Ed., Academic Press, Inc., New York, (1985), p. 153.
25. S. Aisenberg, R. Chabot, J. Appl. Phys., Vol. 42, (1971), p. 2953.
26. A. Grill, B. Meyerson, *Synthetic Diamond: Emerging CVD Science and Technology*, K. E. Spear and J. P. Dismukes, Eds., John Wiley & Sons, Inc., New York, (1994), p. 91.
27. J. Ishikawa, K. Ogawa, K. Miyata, T. Takagi, Nucl. Instrum. Methods, Vol. B21, (1987), p. 205.
28. F. Rossi, B. Andre, in Proc. IP AT 1991, Brussels, CEP Consultants, Edinburgh, UK, (1991), p. 43.

Figure Captions

Figure 1. The experimental set up comprising a microwave discharge cell operated under flow conditions.

Figure 2. The positive ion ToF-SIMS spectra ($m/e = 0-800$) of a noncoated cleaned commercial silicon wafer.

Figure 3. The positive ion ToF-SIMS spectra ($m/e = 0-200$) of a cleaned commercial silicon wafer coated by reaction of a helium-hydrogen plasma with CH_4 as the source of C that showed a large H^+ peak and trace hydrocarbon fragments $C_xH_y^+$.

Figure 4. The negative ion ToF-SIMS spectrum ($m/e = 0-800$) of a noncoated cleaned commercial silicon wafer.

Figure 5. The negative ion ToF-SIMS spectrum ($m/e = 0-200$) of a cleaned commercial silicon wafer coated by reaction of a helium-hydrogen plasma with CH_4 as the source of C that was dominated by hydride ion (H^-) and carbon ion (C^-). Very little oxide (O^-) or hydroxide (OH^-) was observed. An exceptional feature was the multimeric carbon clusters C_x^- at $m/e = 12,24,36,48,60,72,96,108,120$.

Figure 6. The XPS survey scan of a cleaned commercial silicon wafer. Only silicon, oxygen, and trace carbon contamination were observed.

Figure 7. The XPS survey scan of a cleaned commercial silicon wafer coated by reaction of a helium-hydrogen plasma with CH_4 as the source of C. Only carbon and trace silicon and oxygen contamination were observed.

Figure 8. High resolution XPS spectra (0-35 eV) of the valence band region of (a) single crystal diamond, (b) diamond film, (c) glassy carbon, (d) pyrolytic graphite, (e) mineral graphite, and (f) HDLC.

Figure 9. High resolution XPS spectra (0-35 eV) of the valence band region of a cleaned commercial silicon wafer coated by reaction of a helium-hydrogen plasma with CH_4 as the source of C that showed features that matched single crystal diamond.

Figure 10. High resolution XPS spectra (280-340 eV) of the $C\,1s$ energy loss region of (a) single crystal diamond, (b) diamond film, (c) glassy carbon, (d) pyrolytic graphite, (e) mineral graphite, and (f) HDLC.

Figure 11. High resolution XPS spectrum (280-340 eV) of the $C\,1s$ energy loss region of a cleaned commercial silicon wafer coated by reaction of a helium-hydrogen plasma with CH_4 as the source of C that showed features that matched single crystal diamond.

Figure 12. The Raman spectrum recorded on the diamond film. The diamond band, D-band, G-band of DLC, and G-band of graphite were observed at 1323.5 cm^{-1}, 1327.0 cm^{-1}, 1484.0 cm^{-1} and 1591.6 cm^{-1}, respectively. The 19.6 cm^{-1} FWHM of the diamond peak is characteristic of and identified the film as having single crystal diamond.

Figure 13. The Raman spectrum of a second diamond film formed by helium-hydrogen-methane (48.2/48.2/3.6%) microwave discharge plasma CVD. A diamond band was observed at 1332 cm^{-1} . In addition, the G-band of graphite was observed at 1580.

Figure 14. The X-ray Diffraction (XRD) pattern of a diamond film for 2θ = 10° to 100°. The dominant peaks were due to silicon of the substrate. Diamond peaks (D) were observed at 2θ = 43.9° (111) and 75.3° (220).

Figure 15. The visible spectrum (275-700 nm) recorded on a helium-hydrogen-methane microwave discharge plasma. CH, C_2, and C_3 emission were observed with significantly broadened H α, β, and γ lines.

Figure 16. The 656.3 nm Balmer α line width recorded with a high resolution ($\pm 0.006\,nm$) visible spectrometer on a xenon-hydrogen (90/10%) (solid curve) and a hydrogen microwave discharge plasma (dotted curve). No line excessive broadening was observed from either plasma corresponding to an average hydrogen atom temperature of $2-3\,eV$.

Figure 17. The 656.3 nm Balmer α line width recorded with a high resolution ($\pm 0.006\,nm$) visible spectrometer on a helium-hydrogen (90/10%) and a hydrogen microwave discharge plasma. Significant broadening was observed for the helium-hydrogen plasma corresponding to an average hydrogen atom temperature of $180-210\,eV$ compared to $2-3\,eV$ for a hydrogen plasma.

Figure 18. The 656.3 nm Balmer α line width recorded with a high resolution ($\pm 0.006\,nm$) visible spectrometer on helium-hydrogen-methane (48.2/48.2/3.6%) and hydrogen-methane (10/90%) microwave discharge plasmas. Significant broadening was observed for the helium-hydrogen-

methane plasma corresponding to an average hydrogen atom temperature of 120-140 eV compared to 2-3 eV for a hydrogen-methane plasma.

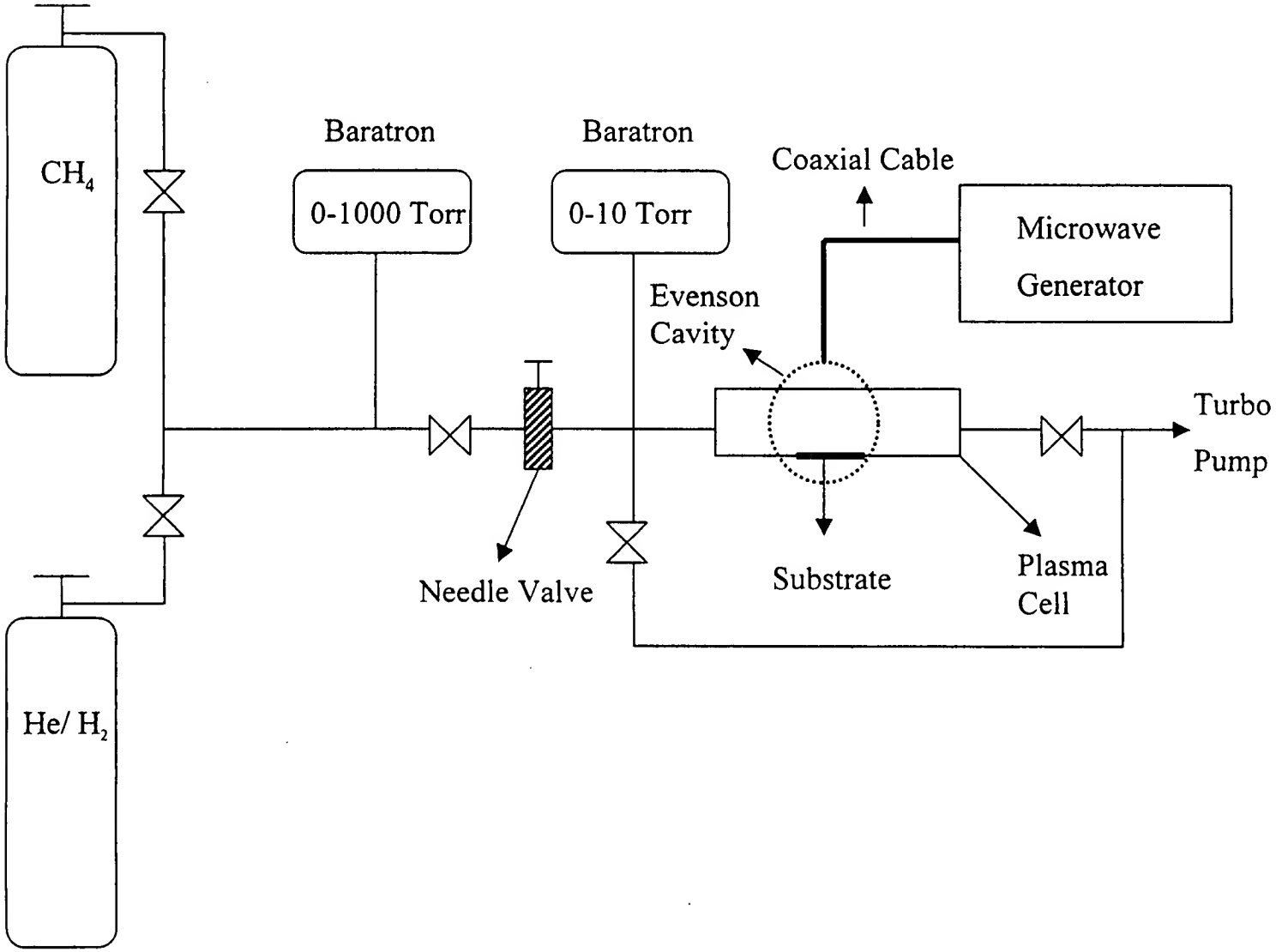
CH_4
Baratron
0-1000 Torr
Baratron
0-10 Torr
Coaxial Cable
Microwave
Generator
Evenson
Cavity
Turbo
Pump
Needle Valve
Substrate
Plasma
Cell
He/ H_2

Fig. 1

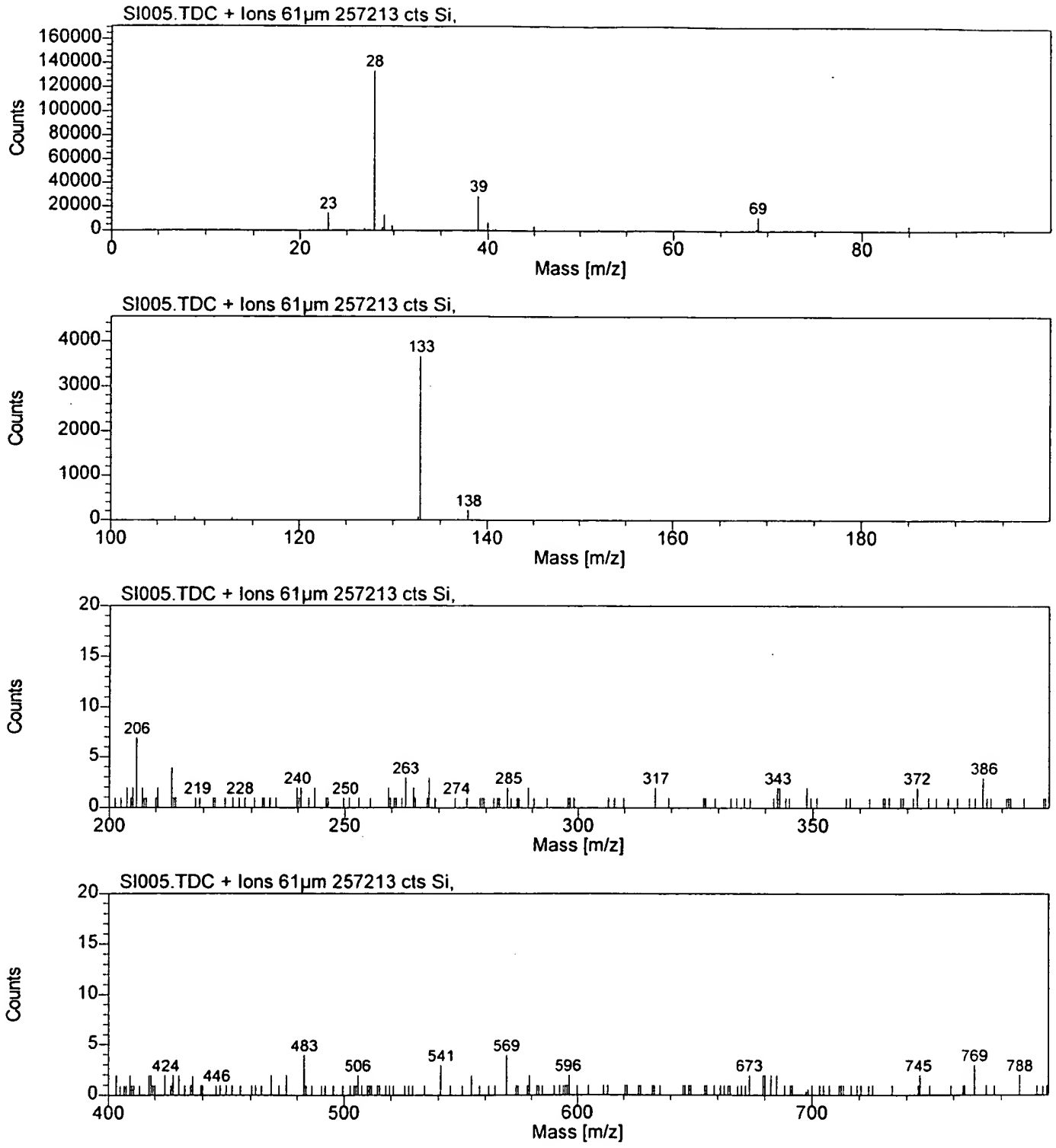
SI005.TDC + Ions 61µm 257213 cts Si,
Counts
Mass [m/z]
28
23
39
69
133
138
206
219
228
240
250
263
274
285
317
343
372
386
424
446
483
506
541
569
596
673
745
769
788

Fig. 2

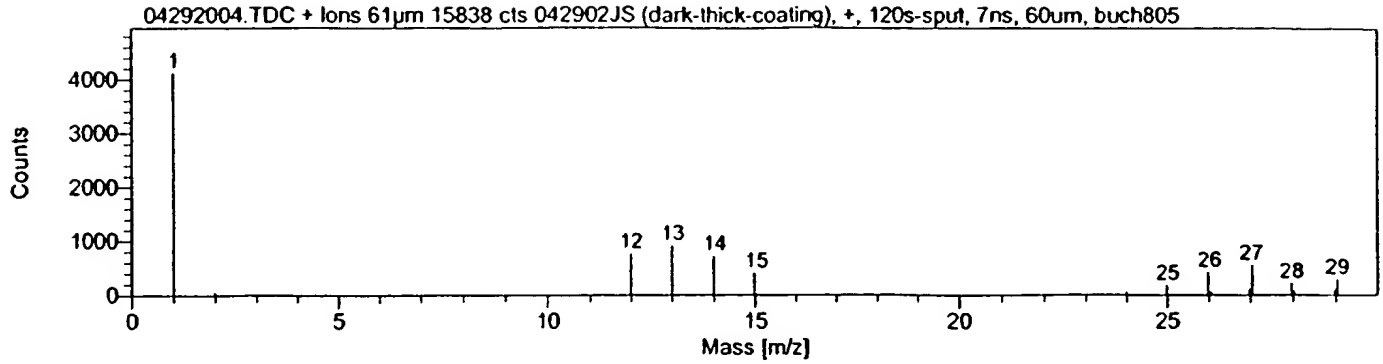
04292004.TDC + Ions 61µm 15838 cts 042902JS (dark-thick-coating), +, 120s-sput, 7ns, 60um, buch805
Counts
Mass [m/z]
1
12
13
14
15
25
26
27
28
29

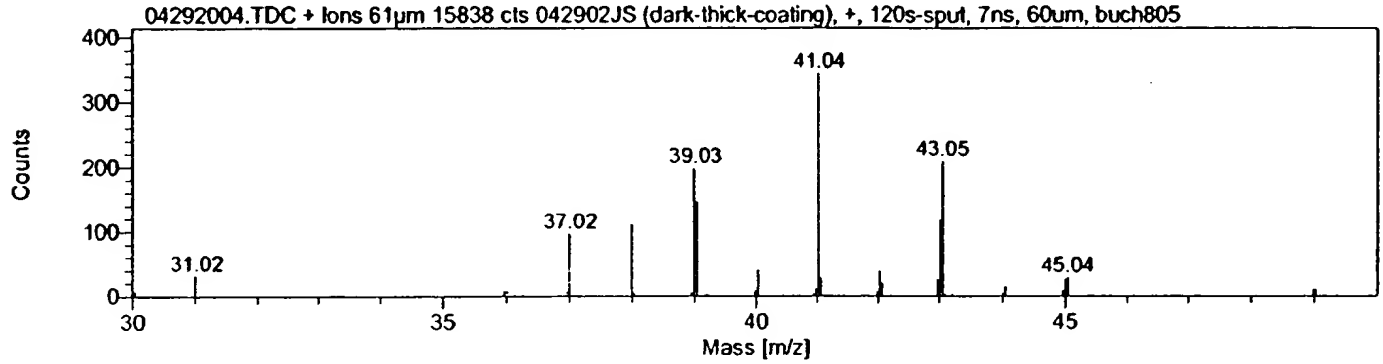
04292004.TDC + Ions 61µm 15838 cts 042902JS (dark-thick-coating), +, 120s-sput, 7ns, 60um, buch805
Counts
Mass [m/z]
41.04
39.03
43.05
37.02
31.02
45.04

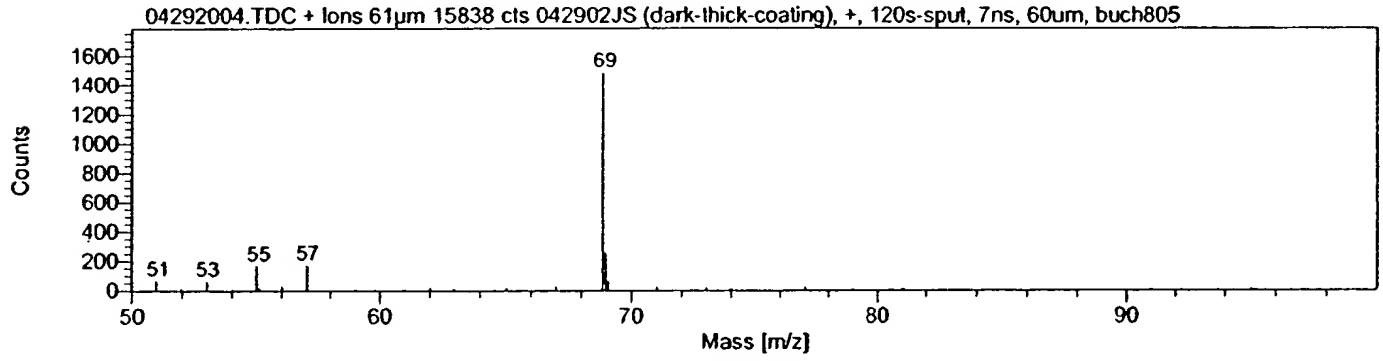
04292004.TDC + Ions 61µm 15838 cts 042902JS (dark-thick-coating), +, 120s-sput, 7ns, 60um, buch805
Counts
Mass [m/z]
69
51
53
55
57

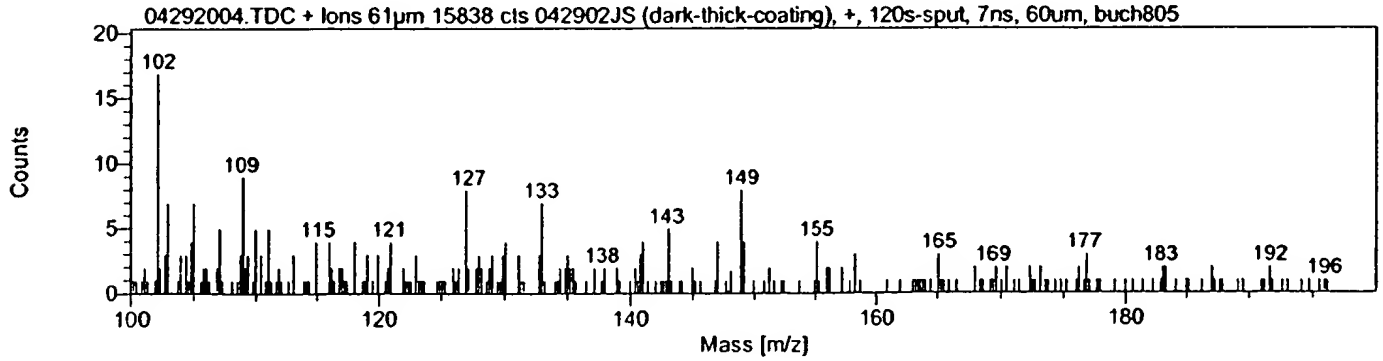
04292004.TDC + Ions 61µm 15838 cts 042902JS (dark-thick-coating), +, 120s-sput, 7ns, 60um, buch805
Counts
Mass [m/z]
102
109
115
121
127
133
138
143
149
155
165
169
177
183
192
196

Fig. 3

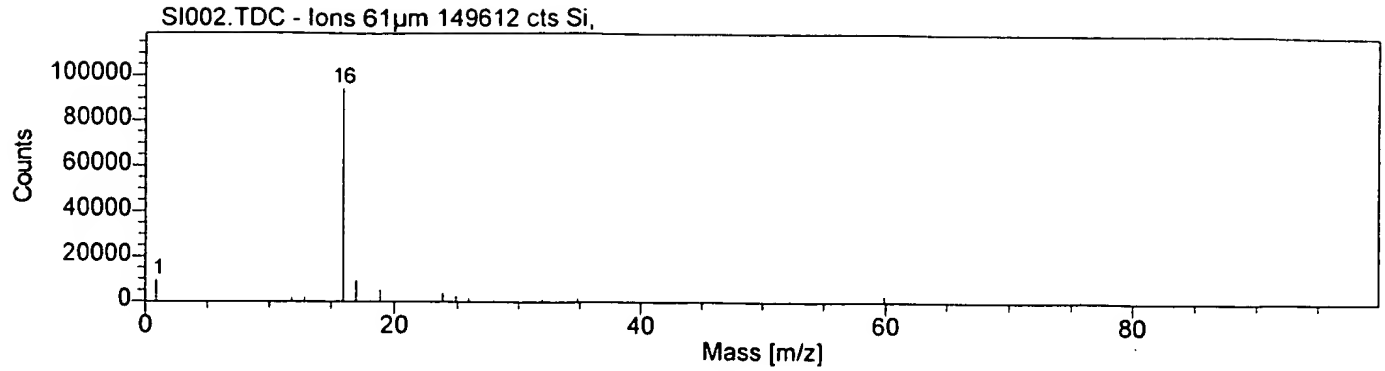
SI002.TDC - Ions 61µm 149612 cts Si,
Counts
100000
80000
60000
40000
20000
0
16
1
0
20
40
60
80
Mass [m/z]

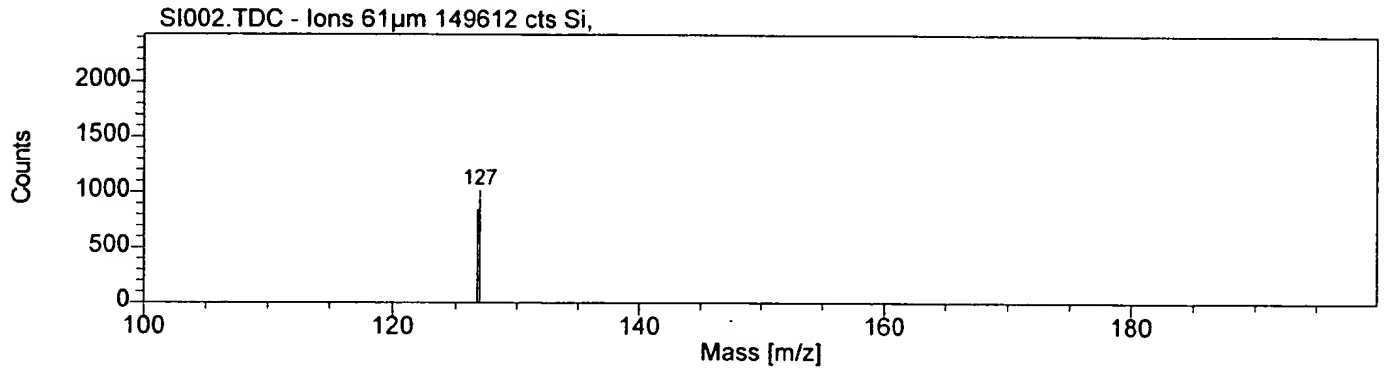
SI002.TDC - Ions 61µm 149612 cts Si,
Counts
2000
1500
1000
500
0
127
100
120
140
160
180
Mass [m/z]

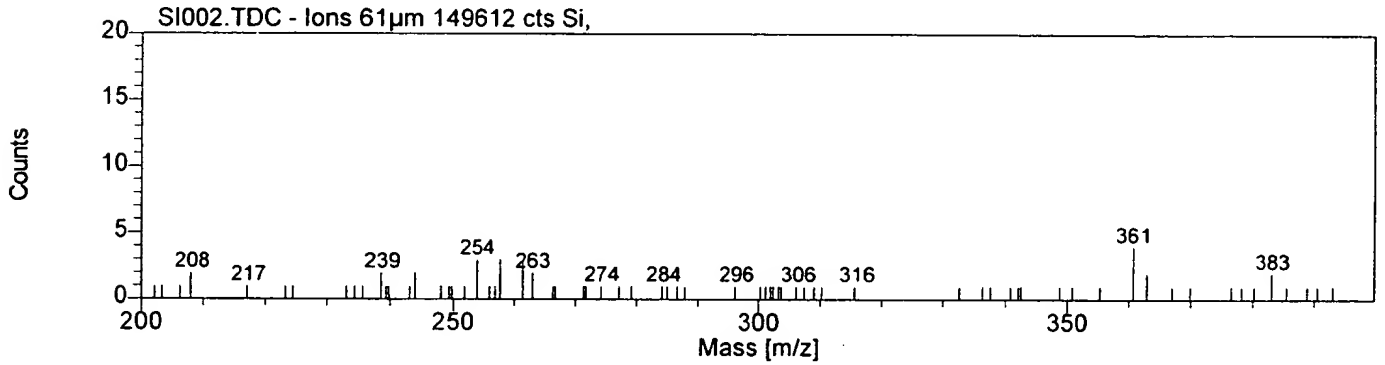
SI002.TDC - Ions 61µm 149612 cts Si,
Counts
20
15
10
5
0
208
217
239
254
263
274
284
296
306
316
361
383
200
250
300
350
Mass [m/z]

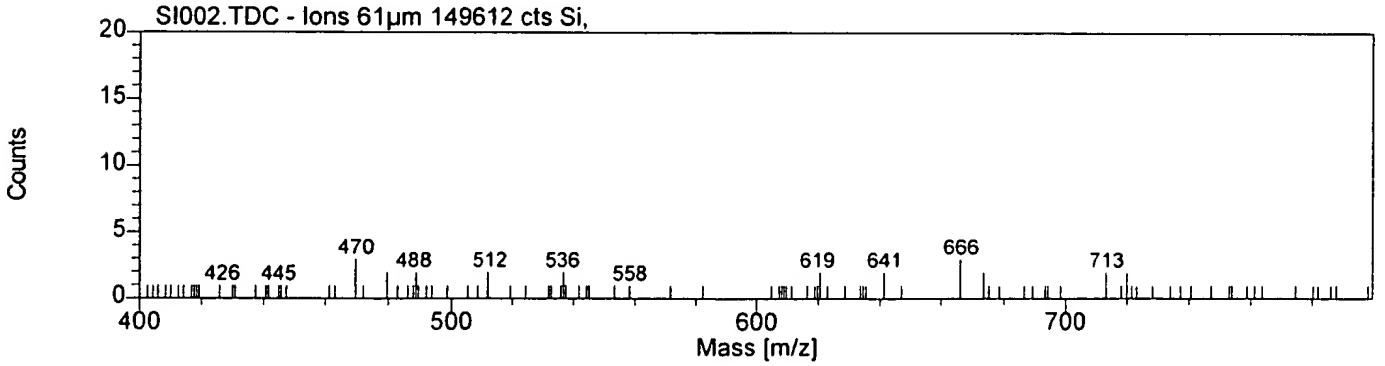
SI002.TDC - Ions 61µm 149612 cts Si,
Counts
20
15
10
5
0
426
445
470
488
512
536
558
619
641
666
713
400
500
600
700
Mass [m/z]

Fig. 4

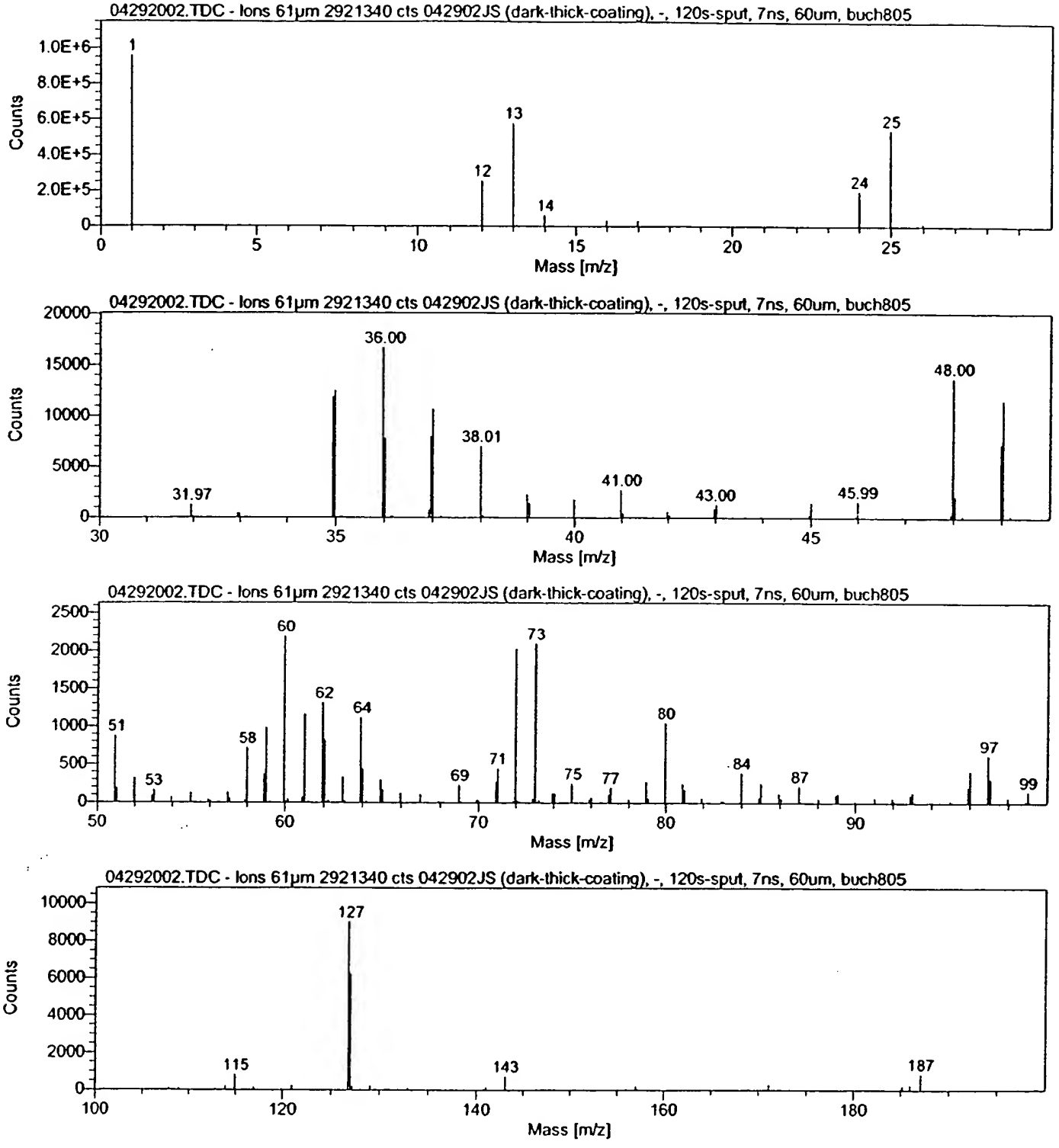
04292002.TDC - Ions 61µm 2921340 cts 042902JS (dark-thick-coating), -, 120s-sput, 7ns, 60um, buch805
Counts
Mass [m/z]
1
12
13
14
24
25
36.00
38.01
31.97
41.00
43.00
45.99
48.00
60
62
64
51
58
53
69
71
73
75
77
80
84
87
97
99
127
115
143
187

Fig. 5

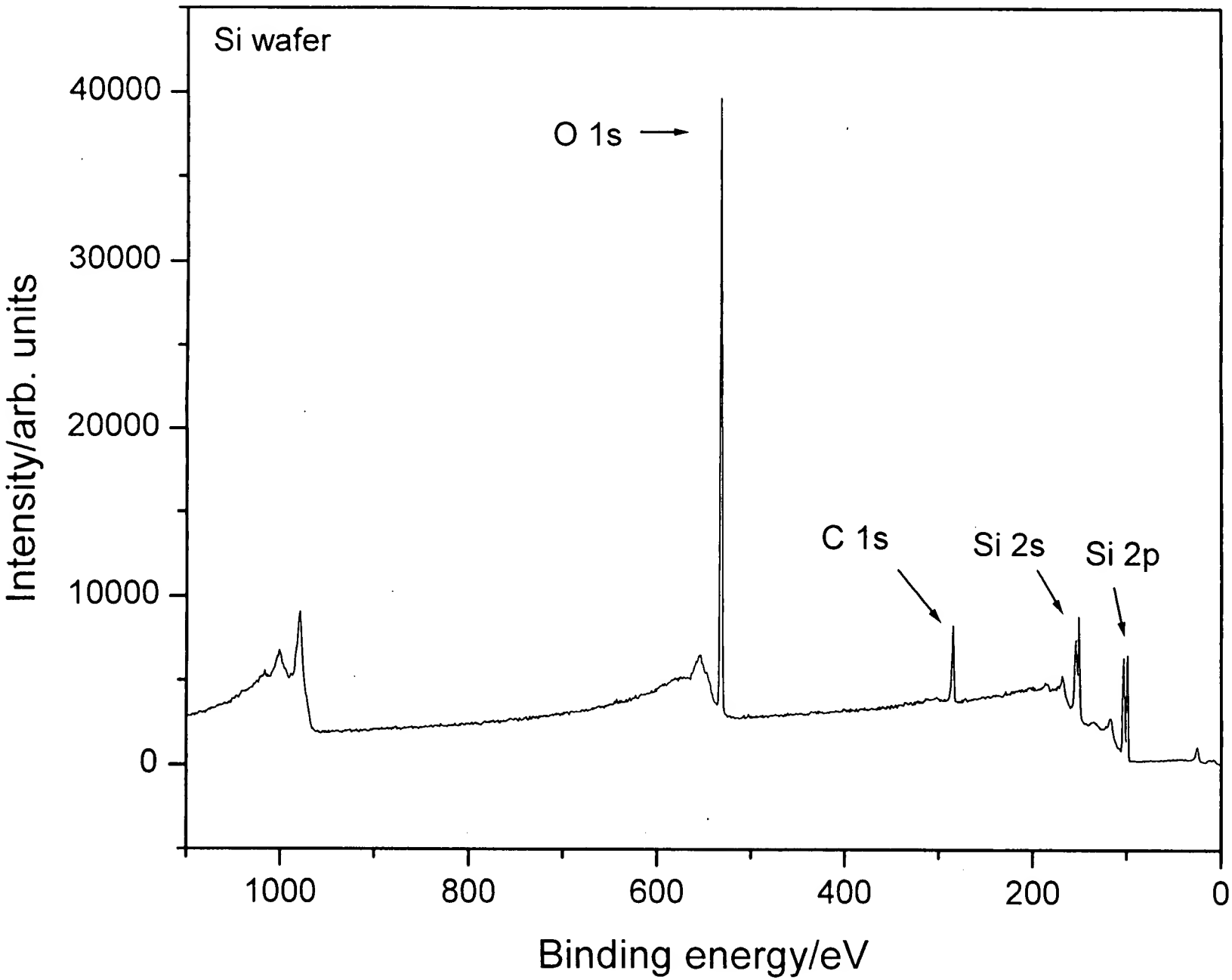
Si wafer
O 1s
C 1s
Si 2s
Si 2p
Intensity/arb. units
40000
30000
20000
10000
0
1000
800
600
400
200
0
Binding energy/eV

Fig. 6

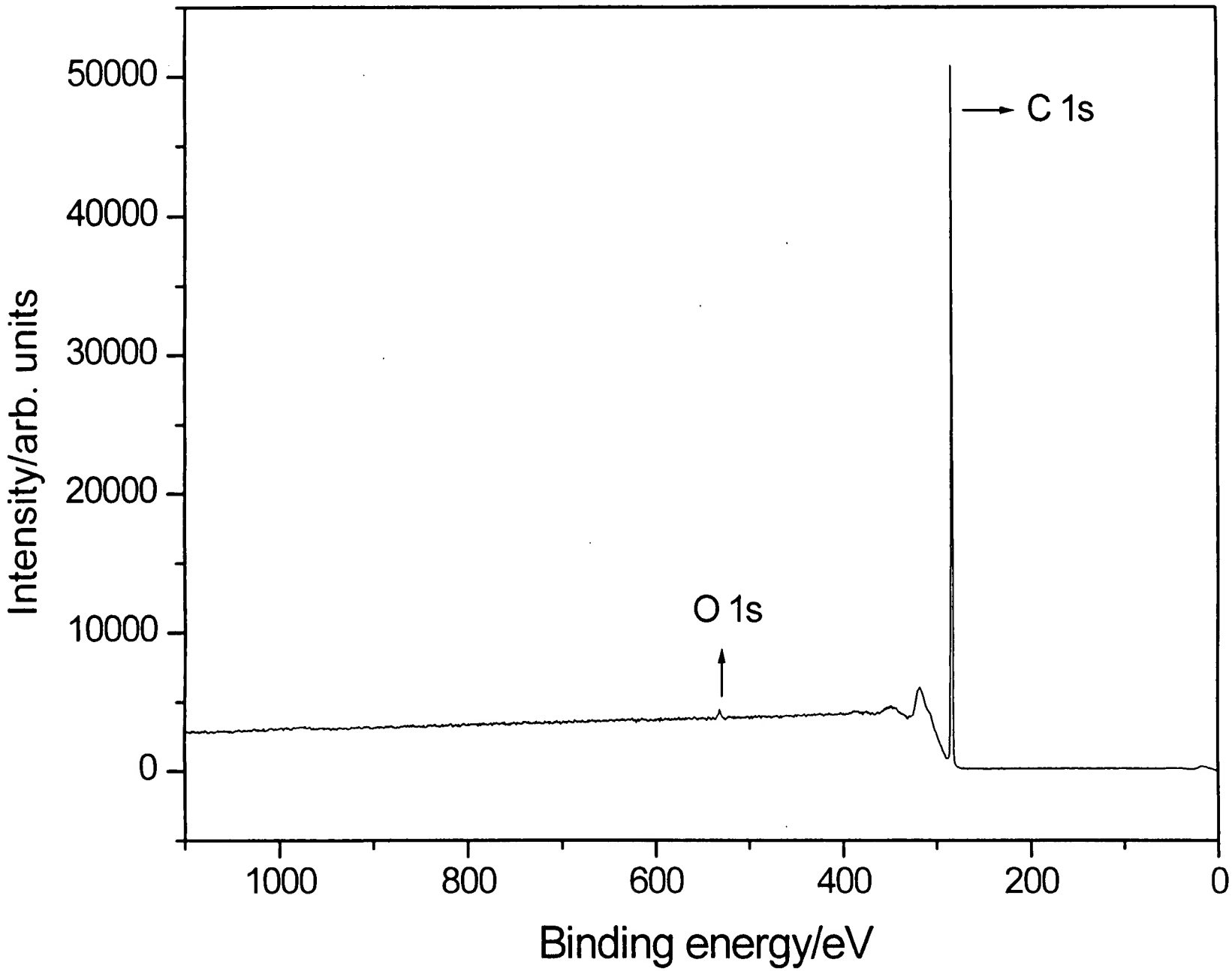
50000
40000
30000
20000
10000
0
Intensity/arb. units
C 1s
O 1s
1000
800
600
400
200
0
Binding energy/eV

Fig. 7

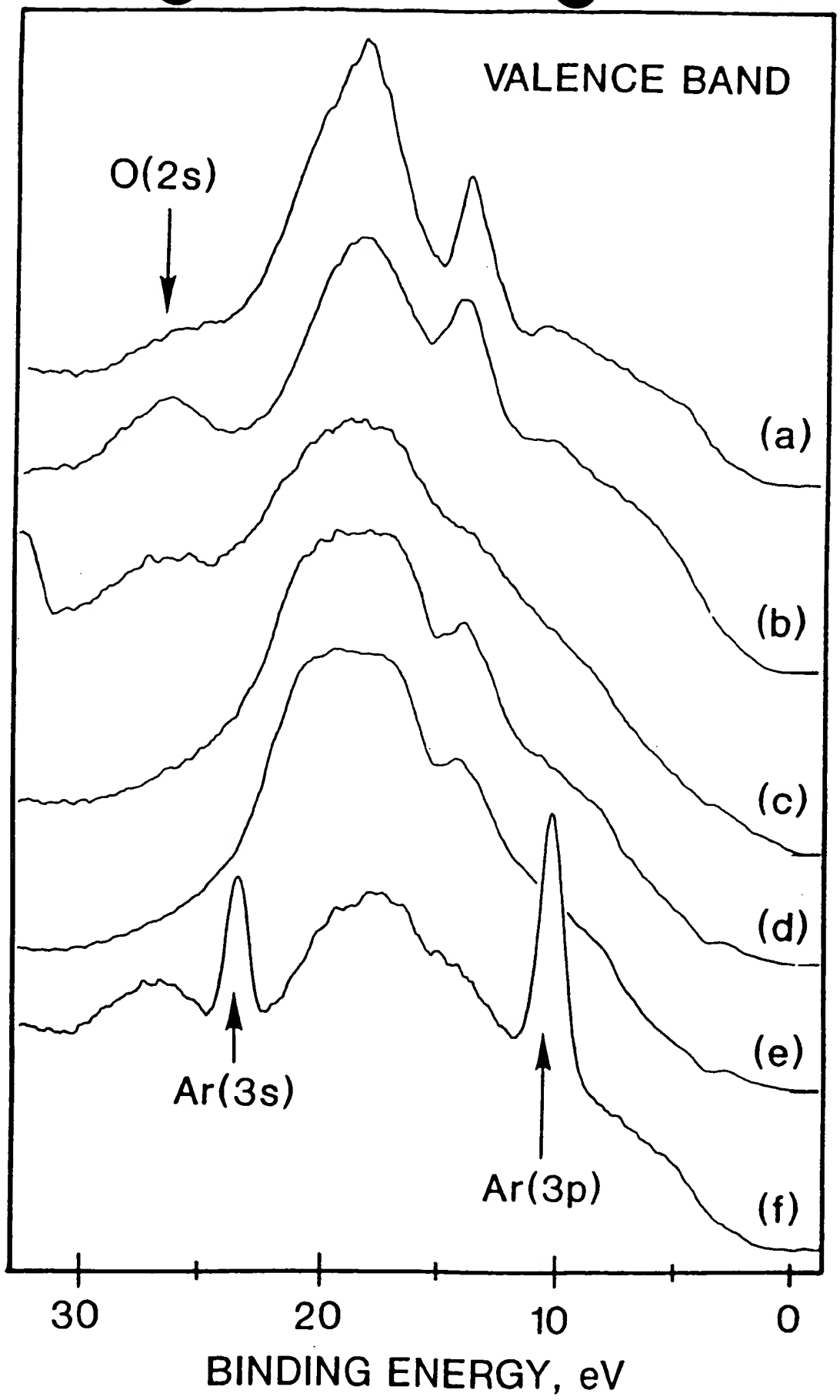
VALENCE BAND
O(2s)
(a)
(b)
(c)
(d)
(e)
(f)
Ar(3s)
Ar(3p)
30
20
10
0
BINDING ENERGY, eV

Fig. 8

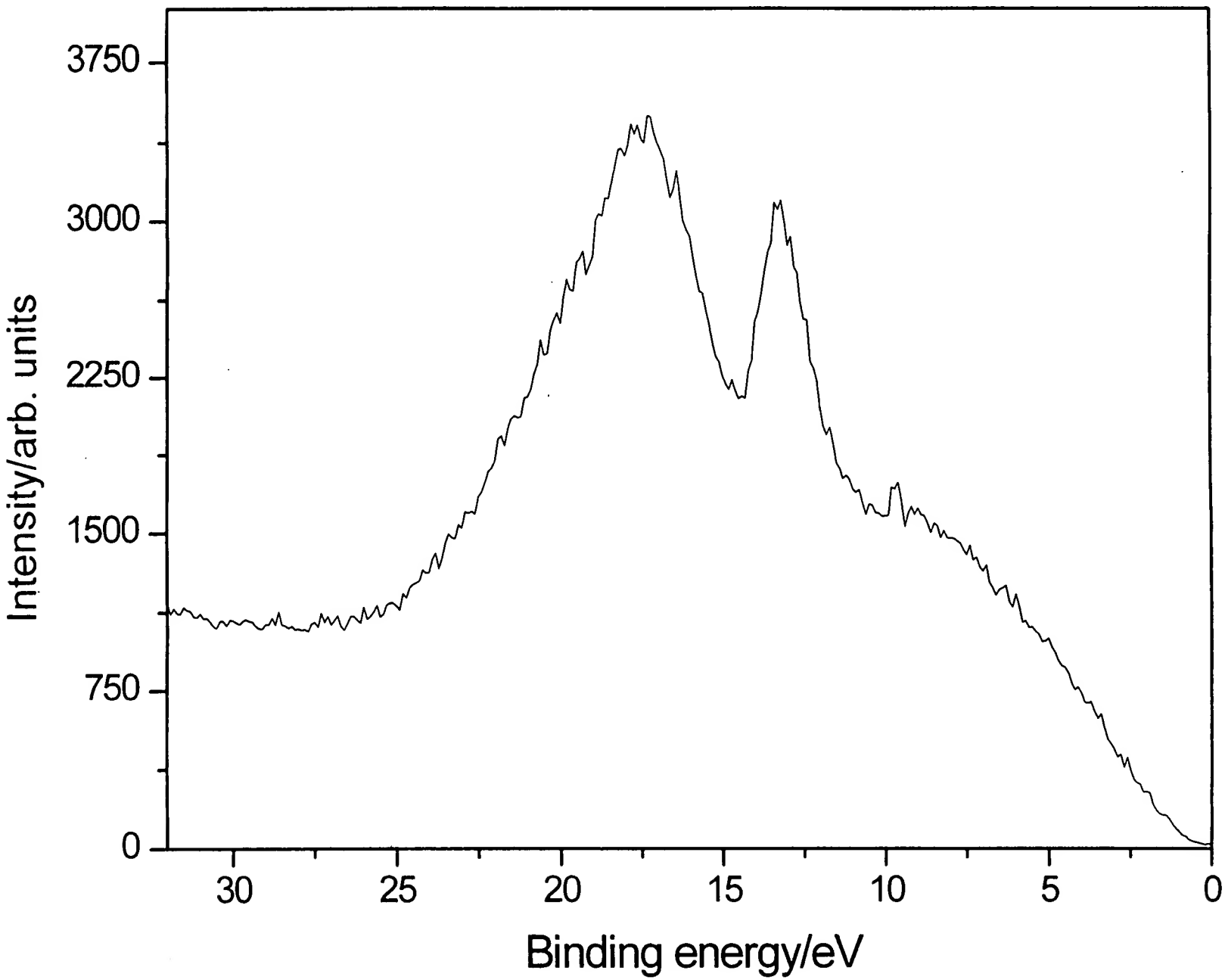
3750
3000
2250
1500
750
0
Intensity/arb. units
30
25
20
15
10
5
0
Binding energy/eV

Fig. 9

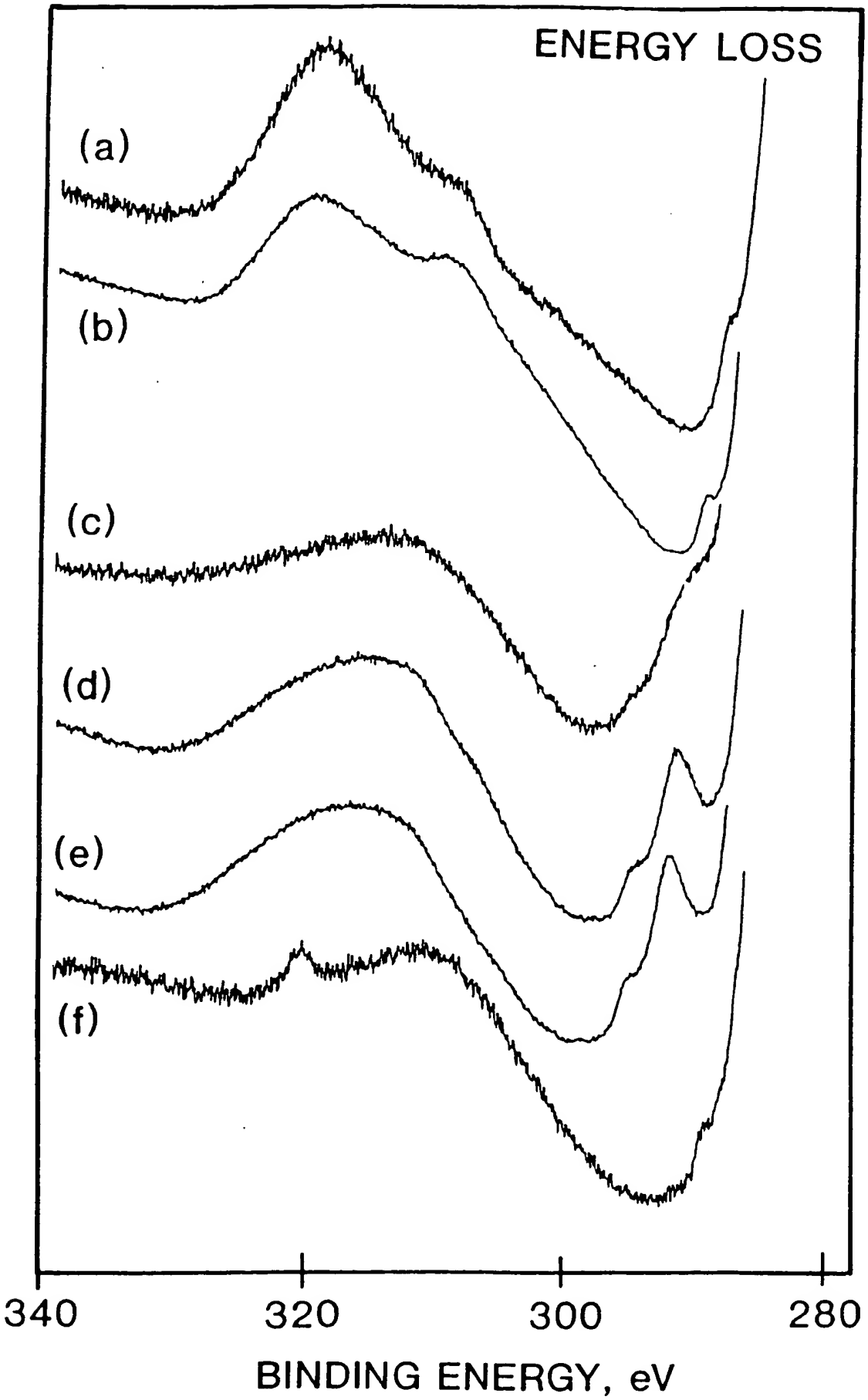

Fig. 10

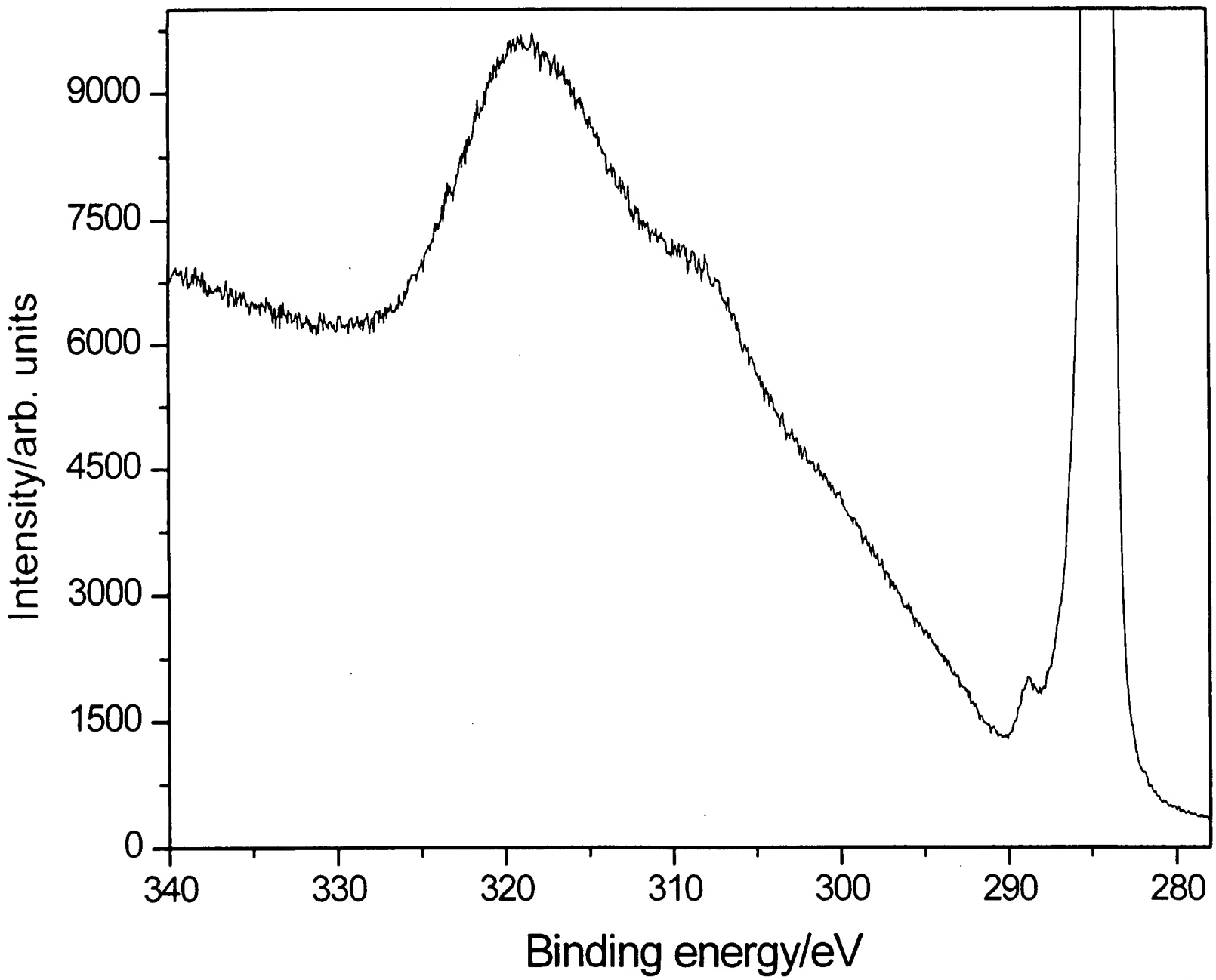
9000
7500
6000
4500
3000
1500
0
Intensity/arb. units
340
330
320
310
300
290
280
Binding energy/eV

Fig. 11

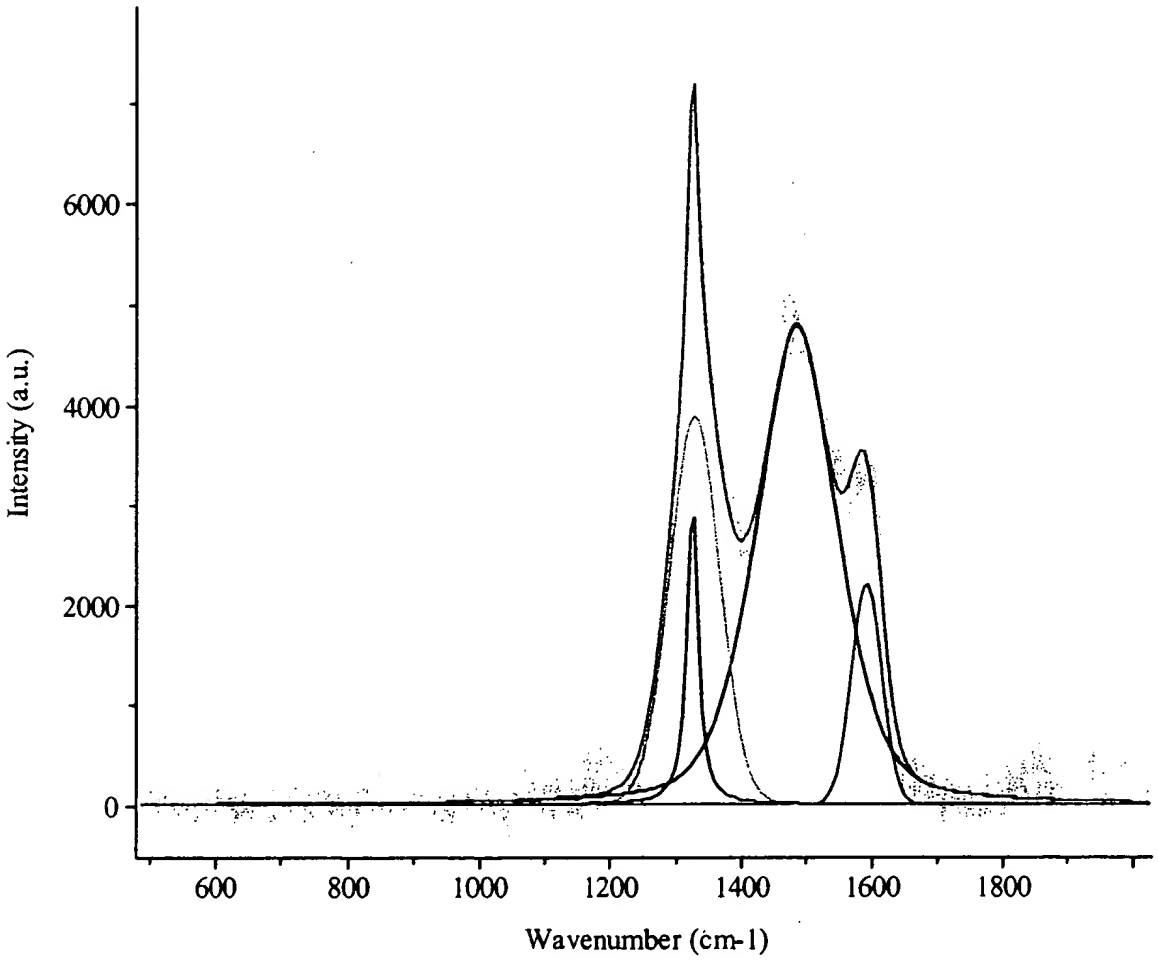
Intensity (a.u.)
6000
4000
2000
0
600
800
1000
1200
1400
1600
1800
Wavenumber (cm-1)

Fig. 12

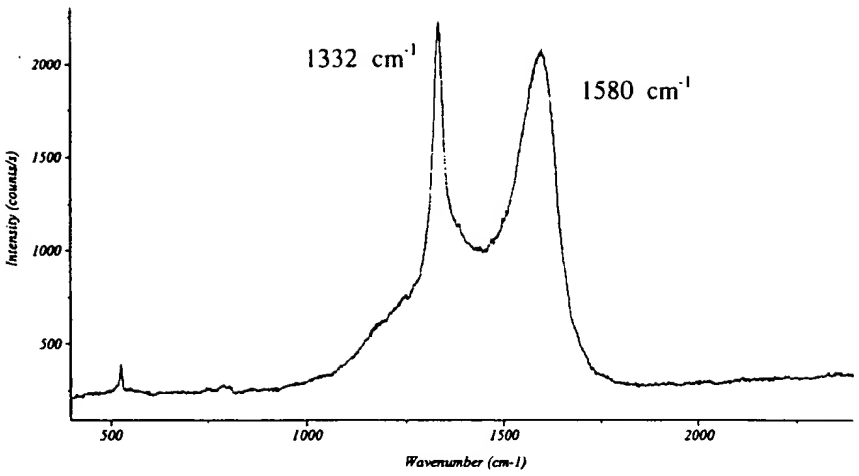
1332 cm-1
1580 cm-1
2000
1500
1000
500
Intensity (counts/s)
500
1000
1500
2000
Wavenumber (cm-1)

Fig. 13

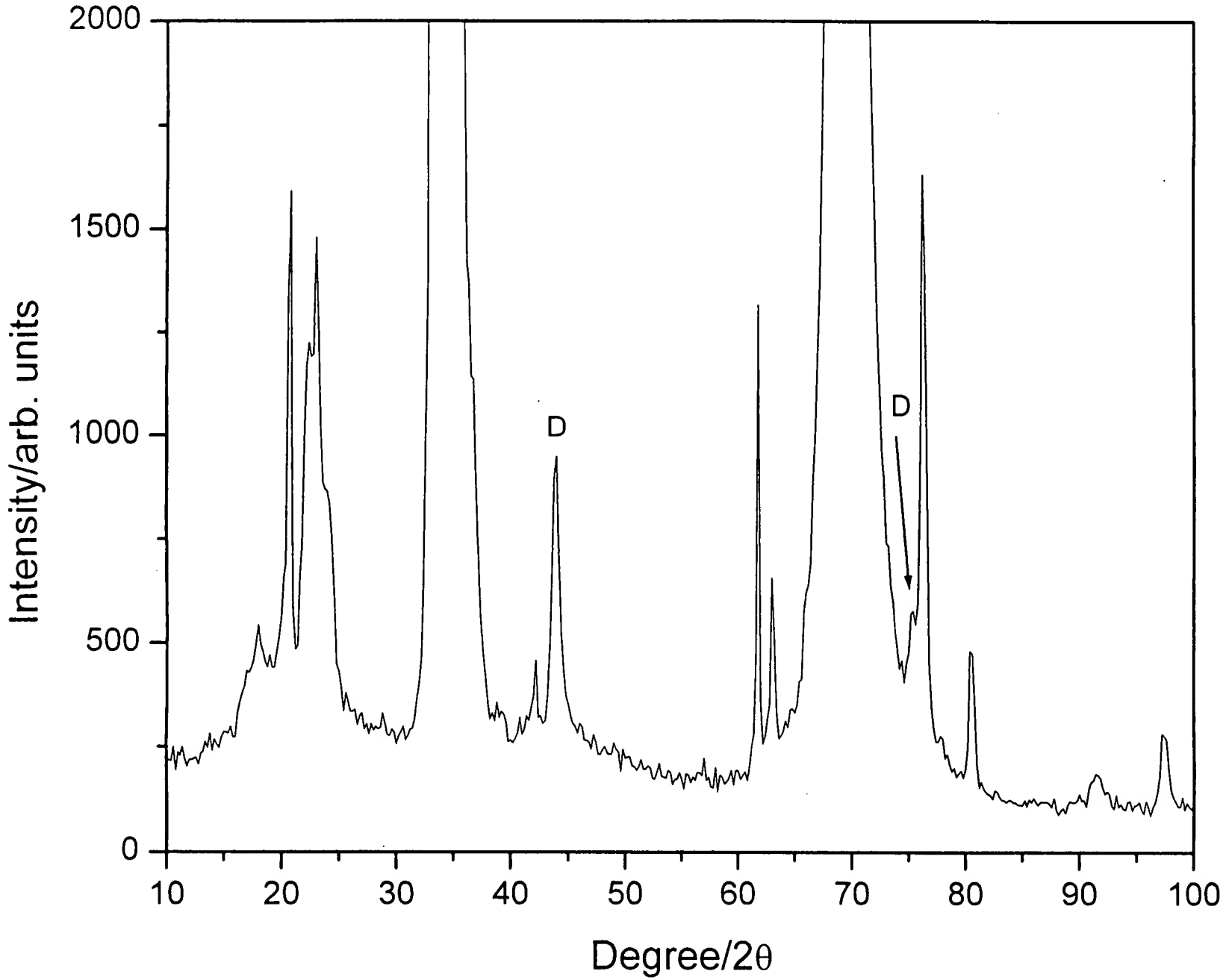
2000
1500
1000
500
0
Intensity/arb. units
D
D
10
20
30
40
50
60
70
80
90
100
Degree/2θ

Fig. 14

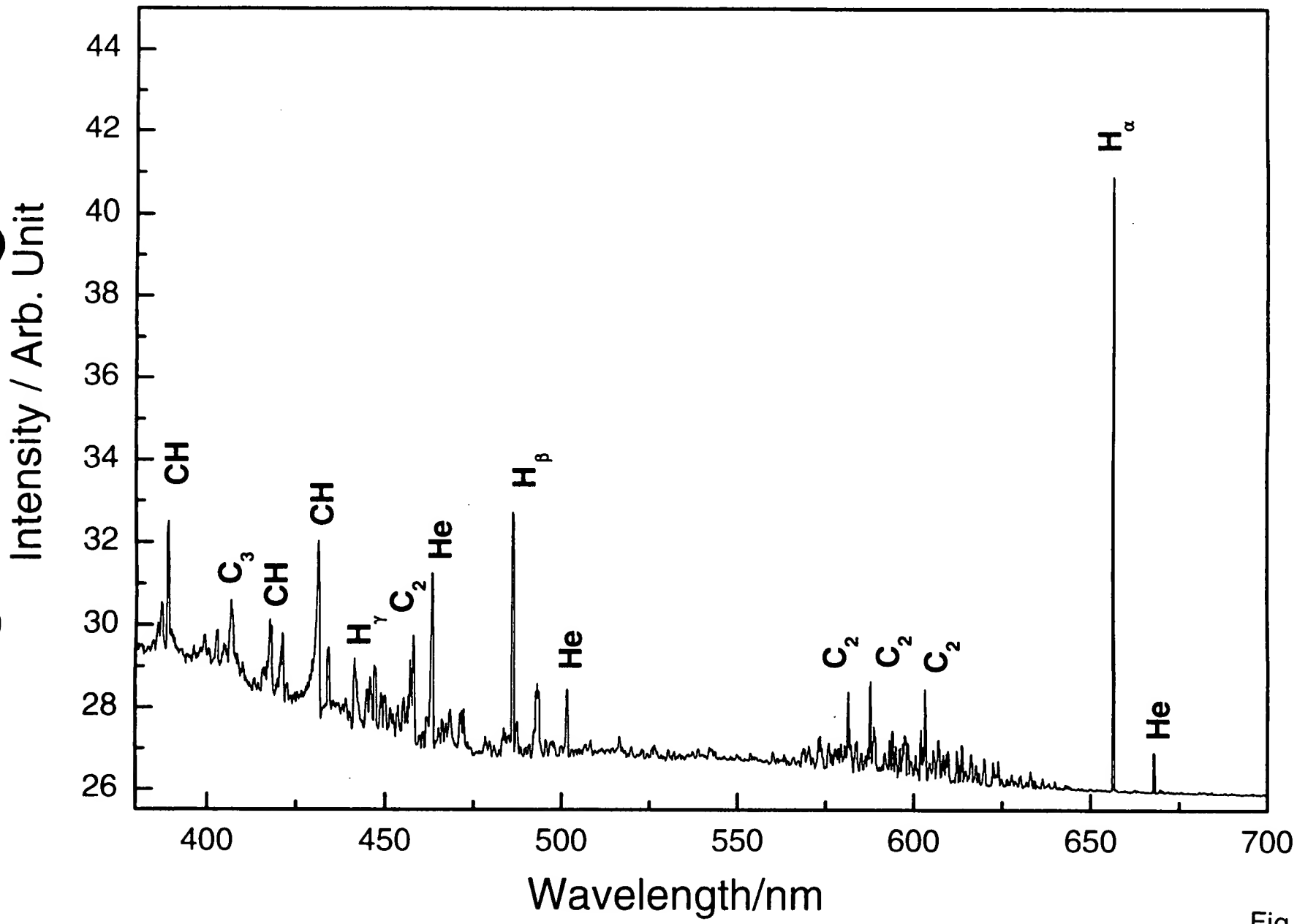
Intensity / Arb. Unit
44
42
40
38
36
34
32
30
28
26
400
450
500
550
600
650
700
Wavelength/nm
CH
C3
CH
CH
Hγ
C2
He
Hβ
He
C2
C2
C2
Hα
He

Fig. 15

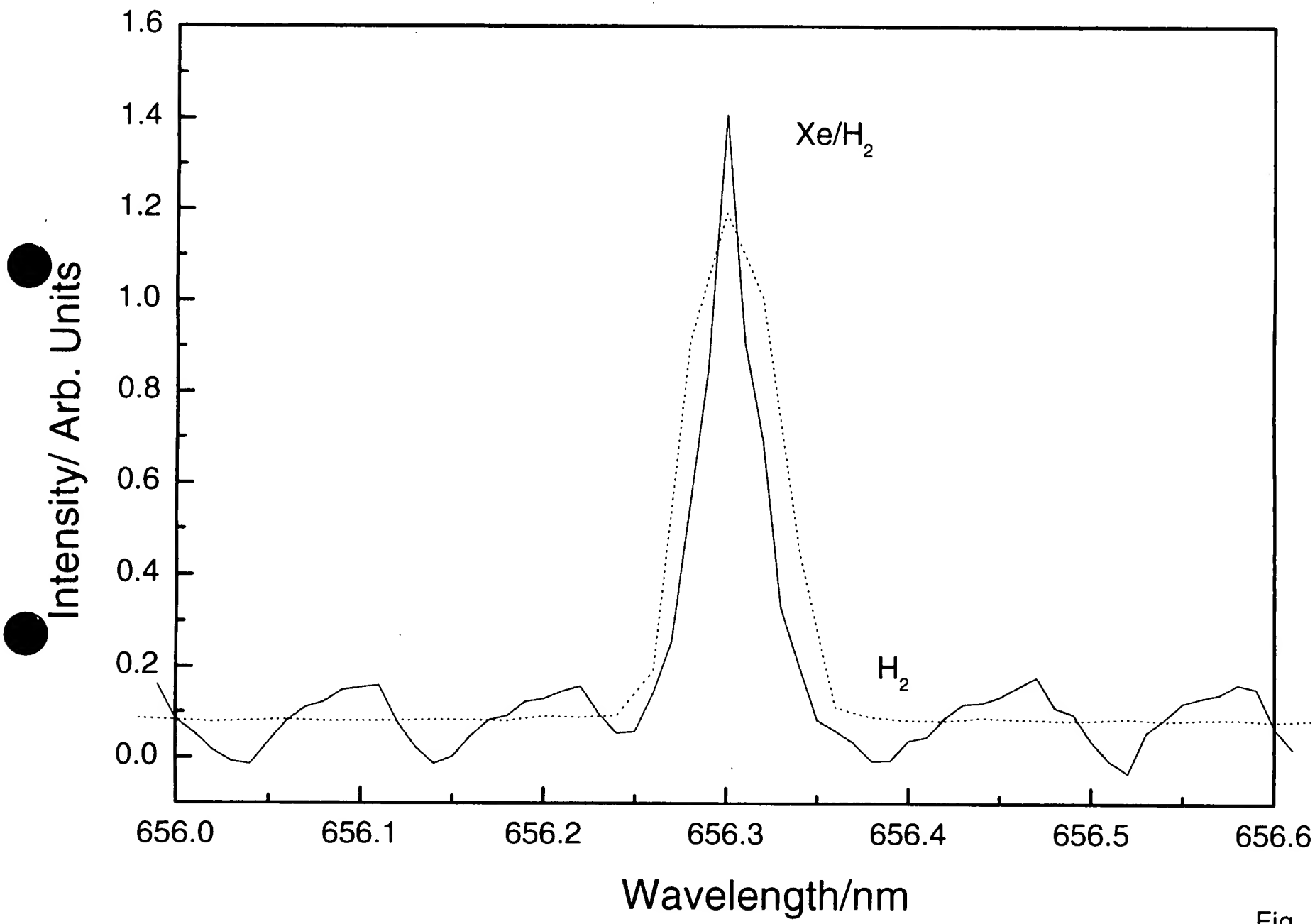
1.6
1.4
1.2
1.0
0.8
0.6
0.4
0.2
0.0
Intensity/ Arb. Units
Xe/H2
H2
656.0
656.1
656.2
656.3
656.4
656.5
656.6
Wavelength/nm

Fig. 16

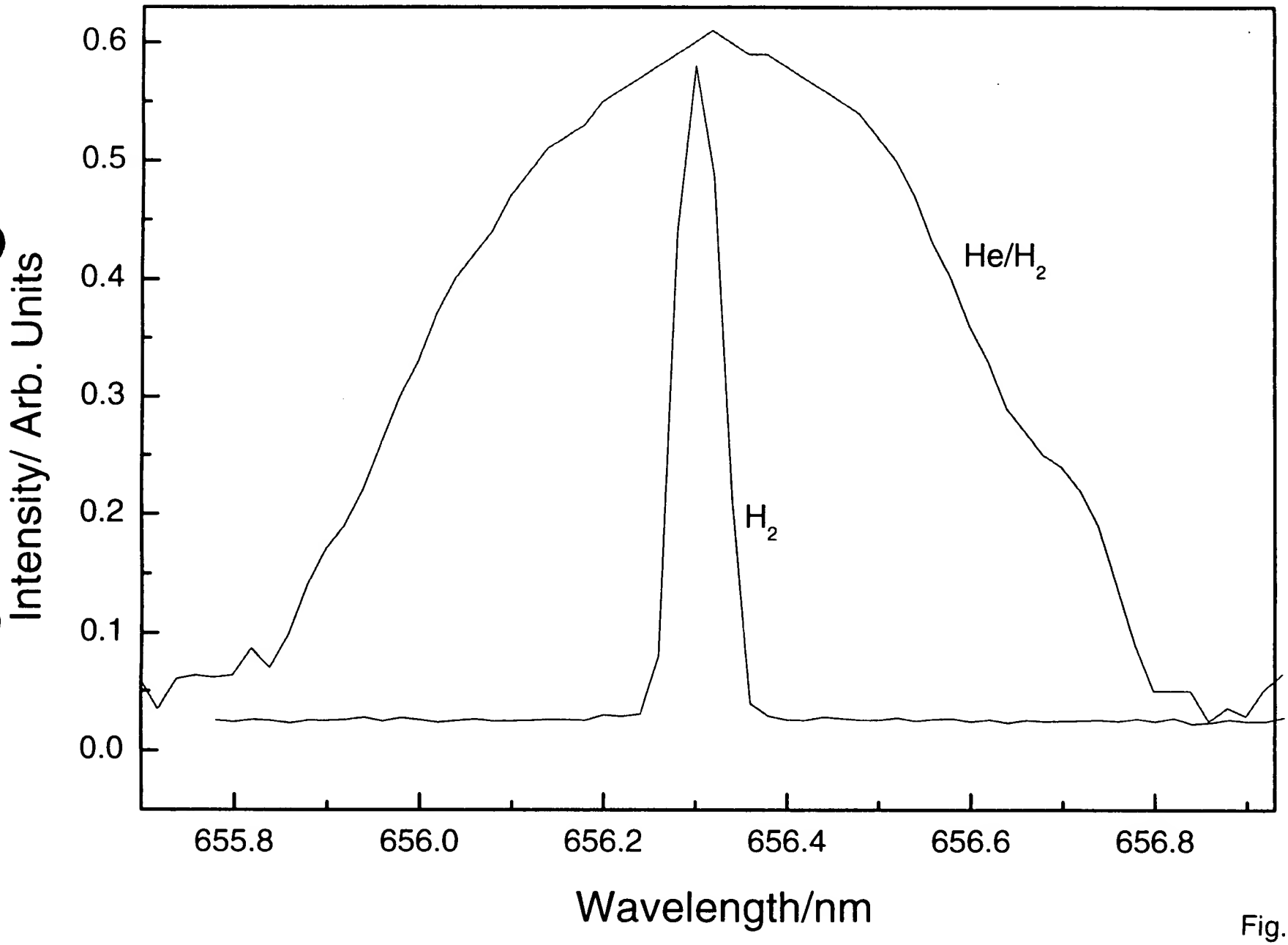
0.6
0.5
0.4
0.3
0.2
0.1
0.0
Intensity/ Arb. Units
He/H2
H2
655.8
656.0
656.2
656.4
656.6
656.8
Wavelength/nm

Fig. 17

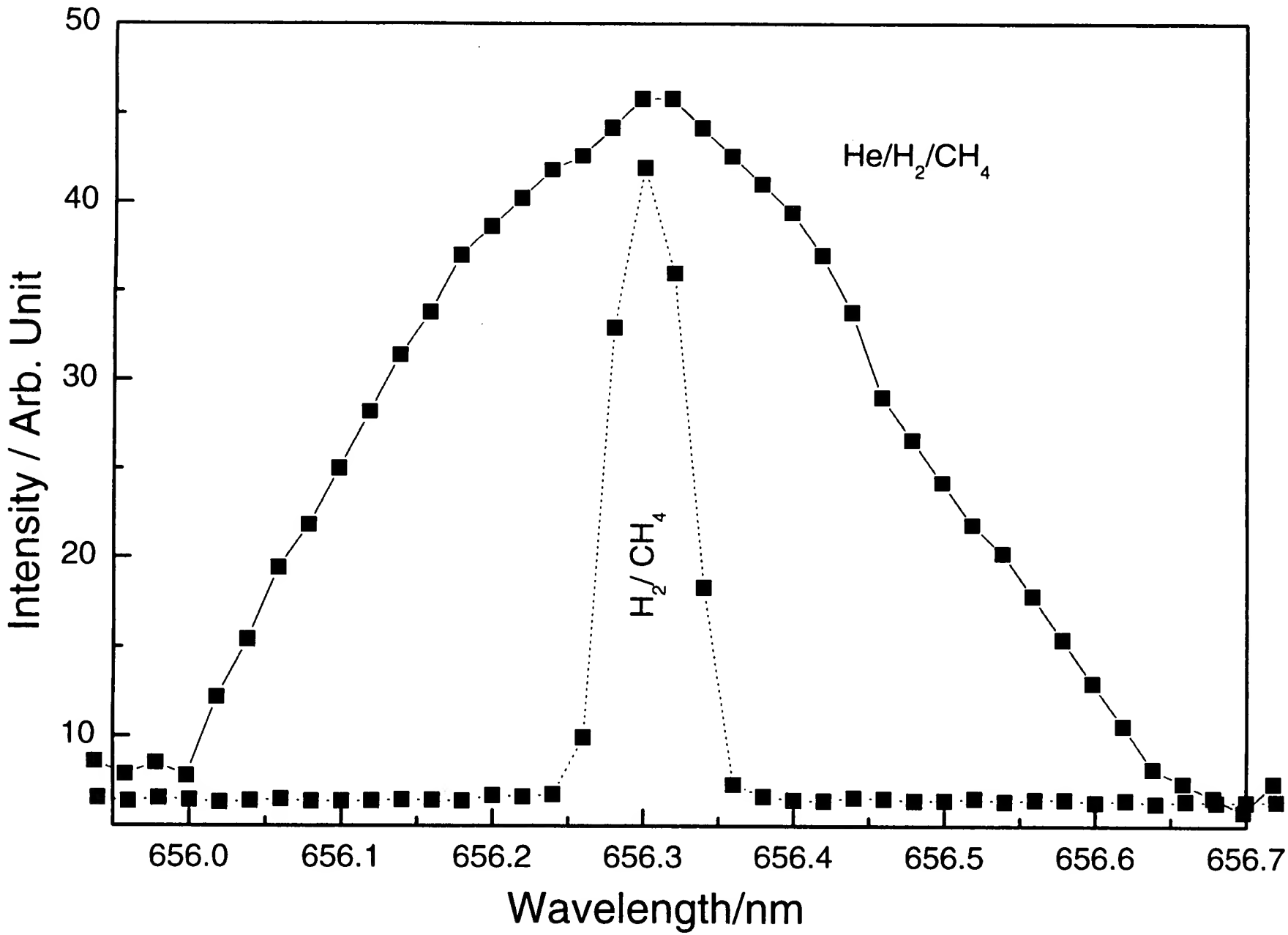
50
40
30
20
10
Intensity / Arb. Unit
He/H2/CH4
H2/CH4
656.0
656.1
656.2
656.3
656.4
656.5
656.6
656.7
Wavelength/nm

Fig. 18